JOURNAL OF PETROLOGY | VOLUME 40 | NUMBER 3 | PAGES 451–473 | 1999

Petrogenesis and Stratigraphy of the High-Ti/Y Urubici Magma Type in the Paraná Flood Basalt Province and Implications for the Nature of 'Dupal'-Type Mantle in the South Atlantic Region

DAVID W. PEATE[1]*, CHRIS J. HAWKESWORTH[2], MARTA M. S. MANTOVANI[3], NICK W. ROGERS[2] AND SIMON P. TURNER[2]

[1]DANISH LITHOSPHERE CENTRE, ØSTER VOLDGADE 10, L, DK-1350 COPENHAGEN K, DENMARK

[2]DEPARTMENT OF EARTH SCIENCES, THE OPEN UNIVERSITY, WALTON HALL, MILTON KEYNES MK7 6AA, UK

[3]DEPARTAMENTO DE GEOFÍSICO, INSTITUTO ASTRONÔMICO E GEOFÍSICO, UNIVERSIDADE DE SÃO PAULO, RUA DO MATÃO 1226, CEP 05508-900, SÃO PAULO SP, BRAZIL

RECEIVED JANUARY 19, 1998; REVISED TYPESCRIPT ACCEPTED AUGUST 13, 1998

The high-Ti/Y Urubici (or Khumib) magma type of the Paraná–Etendeka large igneous province has a restricted spatial extent, near the southeast Brazilian coast and in the northern Etendeka (Namibia). Urubici flows are interbedded with low-Ti/Y Gramado flows. Flow correlations indicate that local topographic relief was important in controlling emplacement of flows, and that lavas near the coast have undergone up to 1 km of post-magmatic uplift relative to inland areas. Urubici magmas have undergone extensive fractional crystallization (MgO <5·5 wt %). Stratigraphic variations highlight complexities of mixing and minor crustal assimilation indicative of open-system magmatic plumbing. The least contaminated samples have high La/Nb (~1·5) and $(Tb/Yb)_N$ (~2·5), Sr–Nd isotopes close to Bulk Earth ($^{87}Sr/^{86}Sr_i$ ~0·7050; ε_{Nd_i} –2·7), and Dupal Pb isotopes with unradiogenic $^{206}Pb/^{204}Pb$ (~17·6). These features are similar to those of the Walvis Ridge DSDP (Deep Sea Drilling Project) Site 525A basalts that define the EM1 oceanic mantle component, and many are also shared with local Cretaceous alkalic magmas that are inferred to be lithospheric mantle melts. Low $^{206}Pb/^{204}Pb$ material found in the Urubici and Site 525A basalts is not seen as a mixing end-member within the modern Tristan plume system or in South Atlantic mid-ocean ridge basalt. An origin from lithospheric mantle material, delaminated and dispersed within the asthenosphere following continental break-up, is preferred. Thus the South Atlantic Dupal mantle anomaly cannot be considered as a single entity: Urubici flood basalts and Walvis Ridge Site 525A basalts have a relatively shallow origin within originally lithospheric mantle, whereas the Tristan plume is a deep mantle upwelling.

KEY WORDS: *Paraná flood basalts; lava stratigraphy; Dupal mantle anomaly; lithospheric mantle; crustal assimilation*

INTRODUCTION

Eruption of the Paraná–Etendeka flood basalt province was associated with the initial opening of the South Atlantic Ocean during the Early Cretaceous. The magmatic history of the Tristan mantle plume can be traced back from its recent activity on the islands of the Tristan group and Gough, along the Rio Grande Rise and the

*Corresponding author. Telephone: (+45) 38 14 2664. Fax: (+45) 33 11 0878. e-mail: dwp@dlc.ku.dk

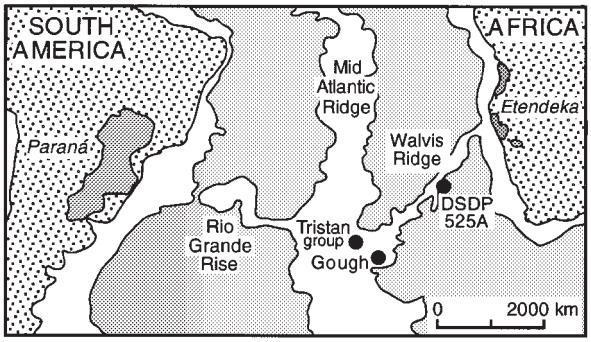

Fig. 1. Map of the South Atlantic region. Shallow features, between 4 km water depth and sea level, are highlighted in white. The magmatic effects of the Tristan mantle plume, whose present location is marked by the Tristan da Cunha island group and Gough island, can be traced back along the Rio Grande Rise and the Walvis Ridge, to the flood basalt exposures of the Paraná and the Etendeka, respectively. The Tristan da Cunha island group also includes Inaccessible and Nightingale islands, which lie 40 km to the WSW and SSW, respectively, of Tristan da Cunha.

Walvis Ridge, to the flood basalt exposures (Fig. 1). The presence of the Tristan plume was clearly an important factor in the generation of the flood basalts, although its exact role is controversial (Morgan, 1981; Fodor, 1987; Hawkesworth *et al.*, 1988; Piccirillo & Melfi, 1988; White & McKenzie, 1989; Peate *et al.*, 1990; Gallagher & Hawkesworth, 1992; Saunders *et al.*, 1992; Arndt *et al.*, 1993; Gibson *et al.*, 1995*a*; Peate & Hawkesworth, 1996; Turner *et al.*, 1996). The issue is whether the basalts were generated by decompressional melting of Tristan plume mantle and/or mid-ocean ridge basalt (MORB)-source asthenospheric mantle, accompanied by some lithospheric contamination, or whether the plume had a more passive role in supplying the heat required to produce the basalts by melting of lithospheric mantle. In a wider context, this issue links to discussions about the nature and location of the 'enriched' mantle components observed in some ocean-island basalts (OIB) and other mantle-derived magmas (e.g. Zindler & Hart, 1986; Hofmann, 1997).

Hawkesworth *et al.* (1986) showed that Paraná flood basalts have Dupal isotope features (high $^{207}Pb/^{204}Pb$ and $^{208}Pb/^{204}Pb$ for a given $^{206}Pb/^{204}Pb$ relative to MORB and OIB from the Northern Hemisphere; Hart, 1984). Most MORB and OIB from the South Atlantic Ocean region between the Paraná and Etendeka flood basalt exposures also show Dupal isotope characteristics. The origin and original location of this isotopically anomalous Dupal mantle is not resolved, with opinion divided between a relatively shallow source in delaminated continental lithospheric mantle material (e.g. Hawkesworth *et al.*, 1986) or a deep source in the lower mantle (e.g. Castillo, 1988). In this paper, we focus on the high-Ti/Y Urubici lavas of southern Brazil because of their compositional similarities (Hawkesworth *et al.*, 1986) to the Deep Sea Drilling Project (DSDP) Site 525A Walvis Ridge samples that Zindler & Hart (1986) used to define their hypothesized EM1 mantle component. Is this an intrinsic component of the Tristan plume or is it lithospheric mantle material that was first sampled during the flood basalt event and then sampled 60 my later along part of the Walvis Ridge as a result of being detached and entrained in the asthenosphere (Richardson *et al.*, 1982; Hawkesworth *et al.*, 1986; Carlson *et al.*, 1996; Milner & le Roex, 1996)?

Extensive flow-by-flow sampling allowed us to determine the lava stratigraphy in detail within a small region on the coastal escarpment (the Serra Geral) of southern Brazil. This provides information about the progressive emplacement of the lava pile, and can help resolve the relative contributions of pre-existing topography and post-magmatic uplift in controlling the present-day configuration of lavas along the coastal escarpment. Temporal variations in composition can provide important clues to the petrogenetic evolution of the Urubici magmas and allow us to estimate better the compositional characteristics of unmodified mantle melts. From these results, we can discuss the mantle origins of the Paraná basalts and the implications for the nature of Dupal mantle in the South Atlantic region.

THE URUBICI MAGMA TYPE AND SAMPLE DETAILS

The Paraná basalts are divided into six distinct compositional magma types (Peate *et al.*, 1992). These are grouped into high-Ti/Y (>310: Urubici, Pitanga, Paranapanema, Ribeira) and low-Ti/Y (<310: Gramado, Esmeralda). The Urubici magma type is volumetrically minor, making up <5% of the total preserved volume of the Paraná lavas (compared with ~50% for the high-Ti/Y Paranapanema and Pitanga magma types: Fig. 2). Its surface extent is restricted to a relatively small strip (~100 km × 350 km) along the north-east flank of the lava field in southern Brazil (Peate *et al.*, 1992). Duncan (1987) found high-Ti/Y flows (Khumib magma type) in the northern part of the formerly adjacent Etendeka lavas of Namibia (Fig. 2), which are compositionally equivalent to the Urubici magma type (e.g. Fig. 3). Despite its small volume, the Urubici magma type is of interest because its Sr–Nd–Pb isotopic composition lies closest, of the high-Ti/Y magma types, to that of the DSDP Site 525A Walvis Ridge basalts that define the EM1 mantle component in the nomenclature of Zindler & Hart (1986).

New compositional data are presented in Tables 1–3 for Urubici samples collected from road profiles traversing the Serra Geral escarpment near São Joaquim (Fig. 4). The Urubici flows are interbedded with low-Ti/Y flows of the Gramado magma type, which have been discussed

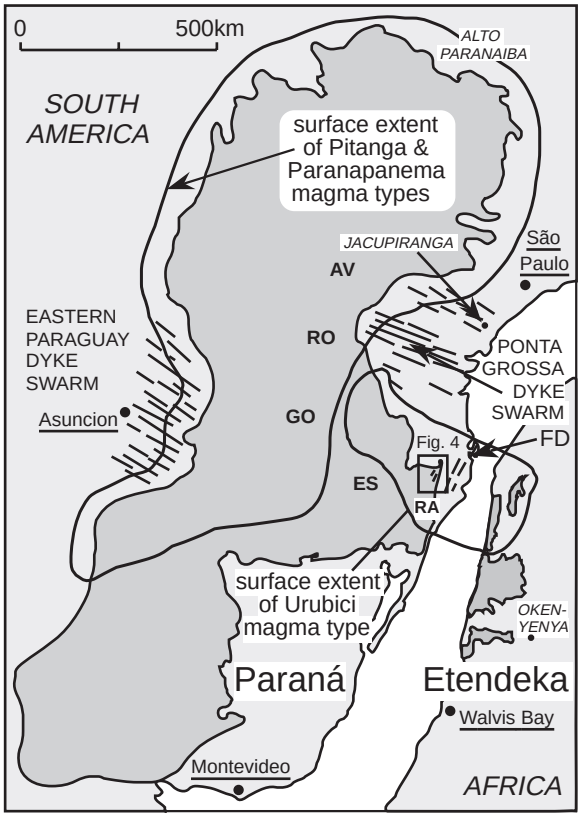

Fig. 2. Pre-drift reconstruction showing the Paraná–Etendeka flood basalt province in relation to the proto-Atlantic rift (Peate *et al.*, 1990). The outlined extents of the high-Ti/Y magma types highlight the difference in erupted volume between the Urubici magma type (including the equivalent Khumib lavas in the Etendeka: Duncan, 1987) and the more extensive Pitanga and Paranapanema lavas (Peate *et al.*, 1992). The box marks the São Joaquim field area, shown in detail in Fig. 4. ES, GO, RO and AV are boreholes where single Urubici samples were recovered at depth (Table 1; Peate *et al.*, 1992). RA is a road profile which contains the southernmost known Urubici flow (Bellieni *et al.*, 1984). FD is the coast-parallel Florianopolis dyke swarm.

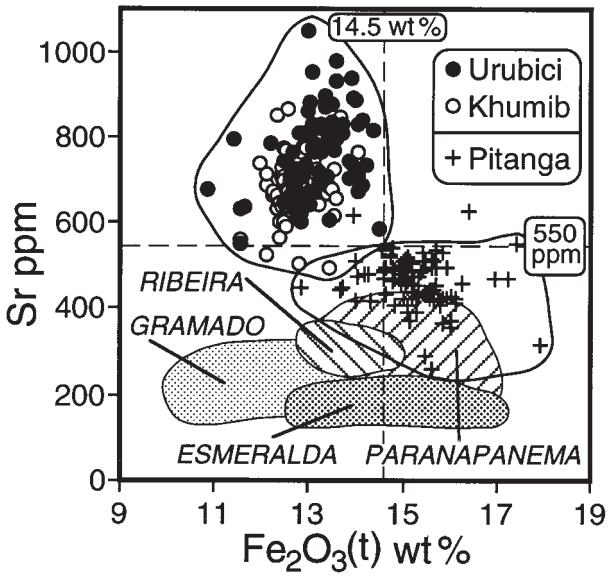

Fig. 3. Fe_2O_3(t) vs Sr diagram. Urubici magma type is defined as samples with TiO_2 >2 wt % that have Sr >550 ppm and Fe_2O_3(t) <14·5 wt %. Values of high-Ti/Y Khumib samples from the Etendeka, Namibia (A. R. Duncan, unpublished data, 1992) overlap completely with the Urubici field. Data for other Paraná basalt magma types from Peate & Hawkesworth (1996) and Peate (1990). Two Pitanga samples with high Sr >550 ppm also have anomalously high Al_2O_3 and have probably accumulated plagioclase.

by Peate & Hawkesworth (1996). The number of Urubici flows within a given profile decreases southwards: none are found south of the RA profile (Fig. 4: Bellieni *et al.*, 1984). Coast-parallel dykes (striking ~NE–SW) of Urubici composition were sampled near the coast at Florianopolis, ~175 km NE of São Joaquim (Fig. 2), and several Urubici dykes of similar orientation were found in the São Joaquim area (Fig. 4).

Urubici samples are subaphyric to weakly porphyritic (<5% phenocrysts) with phenocrysts predominantly of plagioclase and augite. The lavas have a restricted compositional range (MgO = 3·7–5·4 wt %; SiO_2 = 50–53 wt %), with the exception of two andesitic–dacitic flows (DSM-24, 55 wt % SiO_2; DSM-04/08, 60 wt % SiO_2) and one coastal dyke (ST93-5, 55 wt % SiO_2). Urubici and Pitanga basalts have the highest TiO_2 (>3 wt %) and highest incompatible trace element abundances (except for Rb, Ba, Th, K) of the Paraná basalt magma types. Urubici lavas have higher SiO_2, TiO_2, K_2O and lower Fe_2O_3 than Pitanga magmas, at similar MgO contents. Sr and Fe are the most diagnostic elements to distinguish between these two magma types: Urubici magmas have Sr >550 ppm and Fe_2O_3(t) <14·5 wt % (Peate *et al.*, 1992; Fig. 3). Data on coexisting groundmass Ti-magnetite–ilmenite pairs indicate that Urubici magmas equilibrated at lower $f(O_2)$ conditions [close to the QFM (quartz–fayalite–magnetite) buffer] than Pitanga and Paranapanema magmas (~0·5 log units above QFM) (Bellieni *et al.*, 1984).

Urubici magmas have less radiogenic present-day Pb isotope compositions ($^{206}Pb/^{204}Pb$ = 17·4–18·3), lower $^{87}Sr/^{86}Sr_i$, and a more restricted range in $^{87}Sr/^{86}Sr_i$ and ε_{Nd_i} (0·7047–0·7065, and –1·9 to –5·7) than the low-Ti/Y Gramado and Esmeralda magmas (Fig. 5; Peate & Hawkesworth, 1996). Urubici lavas, in common with other Paraná lavas (Hawkesworth *et al.*, 1986; Peate, 1990; Peate & Hawkesworth, 1996) have Dupal Pb isotope compositions, with Δ7/4 >7 and Δ8/4 >85 (Δ7/4 and Δ8/4 are measures of the vertical deviations in $^{207}Pb/^{204}Pb$ and $^{208}Pb/^{204}Pb$ above the Northern Hemisphere Reference Line, a best-fit line to data for MORB and OIB from the Northern Hemisphere; Hart, 1984).

Table 1: XRF major and trace element data for basaltic lavas of the high-Ti/Y Urubici magma type, and selected low-Ti Palmas rhyolites

Sample	Road	Alt. (m)	Flow	SiO_2	TiO_2	Al_2O_3	Fe_2O_3	MnO	MgO	CaO	Na_2O	K_2O	P_2O_5	LOI	V	Co	Ni	Cu	Zn	Ga	Rb	Sr	Y	Zr	Nb	Ba
DGB-09	GB	905	1	52·55	3·59	13·74	12·48	0·15	4·22	7·73	2·78	2·24	0·52	0·56	336	31	52	147	109	25	57	649	37	305	28·0	573
DGB-39	GB	1000	2	51·88	3·79	13·00	13·28	0·17	4·50	8·57	2·52	1·77	0·52	0·25	341	41	65	n.a.	122	23	26	765	35	324	30·0	575
DGB-36	GB	1030	2	52·01	3·67	13·48	13·14	0·17	4·49	8·30	2·49	1·76	0·47	0·93	n.a.	n.a.	48	136	112	25	34	782	36	302	28·7	n.a.
DUP-01	PE	1185	3	51·37	3·89	13·14	13·33	0·18	4·80	9·15	2·50	0·93	0·54	1·39	354	38	57	171	117	26	11	894	39	313	28·4	592
DUP-02	PE	1220	3	50·53	3·89	13·48	13·60	0·18	4·87	8·90	2·85	1·19	0·52	1·98	371	42	60	185	119	25	27	977	43	325	28·6	732
DUP-03	PE	1220	3	50·29	3·95	13·20	14·03	0·18	4·99	8·86	2·60	1·39	0·51	1·80	370	40	59	175	112	25	26	830	39	314	27·3	562
DUP-07	PE	1240	3	49·73	3·74	13·92	13·45	0·16	4·93	8·93	2·69	1·95	0·50	1·65	354	40	56	84	112	32	30	811	40	307	28·8	592
DGB-31	GB	1105	3	50·07	4·00	14·12	14·00	0·16	4·61	9·25	2·20	1·03	0·56	2·31	n.a.	n.a.	40	154	112	27	38	718	43	303	27·8	n.a.
DUP-05	PE	1235	4	52·20	3·55	13·39	13·09	0·18	4·35	8·05	2·68	1·92	0·60	0·75	323	32	36	118	116	24	32	832	38	318	31·3	746
DAB-08	AB	1130	4	51·70	3·60	13·41	12·64	0·16	4·63	8·37	3·19	1·78	0·52	0·08	327	40	91	n.a.	131	25	38	724	44	300	26·0	698
DAB-06	AB	1160	4	51·67	3·63	13·73	13·20	0·17	4·39	7·87	2·82	1·98	0·54	0·15	n.a.	n.a.	39	145	119	24	42	691	41	311	28·9	n.a.
DAB-15	AB	1210	4	51·65	3·61	13·72	13·21	0·17	4·38	7·83	2·96	1·93	0·55	−0·01	n.a.	n.a.	40	154	112	27	38	718	43	303	27·8	n.a.
DUP-04	PE	1230	5	53·00	3·51	13·38	12·76	0·16	4·01	7·39	3·06	2·13	0·60	0·87	323	38	38	134	121	25	34	697	40	326	32·7	686
DUP-06	PE	1235	5	53·52	3·56	13·26	12·87	0·17	4·06	7·45	2·49	2·06	0·54	0·86	332	35	38	125	118	27	34	661	39	322	31·9	690
DAB-10	AB	1190	5	52·83	3·60	13·24	13·02	0·16	4·00	6·91	3·61	2·00	0·63	0·89	295	44	95	n.a.	142	26	43	670	44	335	28·0	817
DGB-25	GB	1175	5	53·74	3·68	12·94	12·94	0·18	3·73	7·26	2·66	2·31	0·56	0·48	344	35	47	163	123	27	47	734	39	351	34·0	816
DUP-46	UR	1190	6	51·40	3·46	12·93	12·86	0·16	4·41	7·77	3·64	1·83	0·51	0·82	330	33	47	152	96	22	43	619	39	301	26·9	457
DSM-37	SM	1235	6	52·53	3·52	13·49	12·68	0·16	4·53	7·55	3·08	1·90	0·57	0·26	331	36	50	132	103	25	44	637	40	310	27·9	785
DSM-36	SM	1260	6	52·48	3·52	13·42	12·81	0·17	4·51	7·69	2·99	1·88	0·53	0·06	344	41	49	126	117	23	42	613	40	313	28·0	701
DUP-44	UR	1220	7	51·51	3·36	13·19	12·93	0·19	5·30	8·49	2·89	1·68	0·45	0·91	339	41	92	124	99	22	40	652	39	269	23·3	794
DUP-43	UR	1225	7	50·99	3·34	13·30	12·89	0·17	5·33	9·29	2·78	1·43	0·47	0·56	365	34	78	148	104	23	23	711	35	269	24·6	437
DSM-35	SM	1275	7	51·61	3·39	13·46	12·67	0·17	5·38	8·53	2·74	1·56	0·49	0·70	343	42	99	151	104	26	31	674	38	268	23·7	503
DUP-42	UR	1270	8	51·54	3·35	13·66	12·48	0·16	4·88	8·73	2·83	1·92	0·46	0·27	336	45	66	142	108	23	38	664	34	271	25·7	525
DSM-34	SM	1300	8	51·48	3·40	13·75	13·25	0·19	4·67	8·32	3·08	1·38	0·47	0·85	314	37	54	166	102	23	29	820	34	272	26·8	709
DSM-33	SM	1305	8	50·44	3·44	14·13	12·97	0·18	4·86	8·86	2·91	1·20	0·48	1·06	365	43	60	159	109	26	19	863	37	277	28·2	736
DUP-40	UR	1290	9	52·04	3·50	13·16	12·80	0·18	5·05	8·85	2·50	1·46	0·47	1·08	358	39	67	158	103	25	21	809	34	275	26·1	572
DSM-31	SM	1325	9	51·84	3·60	13·43	12·61	0·19	4·96	8·32	2·89	1·64	0·53	1·10	347	36	60	136	113	22	31	706	39	278	24·0	743
DAB-12	AB	1250	9/10	51·62	3·51	13·35	12·79	0·18	4·92	8·58	2·78	1·76	0·51	0·08	354	49	81	n.a.	126	23	38	701	39	305	28·0	645
DW-21	CO	1275	9/10	52·00	3·62	13·11	12·86	0·16	4·83	8·15	3·10	1·69	0·48	0·49	344	33	63	135	96	23	36	602	35	279	23·8	502
DRR-18	RR	1245	9/10	51·84	3·61	13·31	13·02	0·17	4·88	8·00	2·68	2·02	0·49	0·13	n.a.	n.a.	69	187	115	23	36	643	38	279	25·4	n.a.
DUP-37	UR	1345	10	52·93	3·55	13·02	12·50	0·16	4·81	8·20	2·63	1·70	0·50	1·00	349	35	52	145	109	28	47	745	36	284	25·1	574
DSM-30	SM	1350	10	51·74	3·61	13·22	12·87	0·17	5·01	8·28	2·89	1·71	0·49	0·26	360	38	62	102	104	27	36	657	37	279	25·0	551

Table 1: continued

Sample	Road	Alt. (m)	Flow	SiO_2	TiO_2	Al_2O_3	Fe_2O_3	MnO	MgO	CaO	Na_2O	K_2O	P_2O_5	LOI	V	Co	Ni	Cu	Zn	Ga	Rb	Sr	Y	Zr	Nb	Ba
DSM-29	SM	1375	10	51·41	3·57	13·43	12·63	0·17	5·14	8·38	3·17	1·57	0·55	0·96	355	43	54	152	111	26	33	699	36	282	23·8	550
DSM-40	SM	1405	10	51·66	3·62	13·27	13·13	0·17	4·71	8·42	2·79	1·72	0·49	0·69	357	35	60	136	118	21	36	764	36	300	27·5	600
DUP-35	UR	1365	11	53·01	3·76	12·86	12·68	0·19	4·34	8·30	2·57	1·70	0·58	0·26	343	36	58	267	107	26	30	764	39	307	26·8	600
DUP-36	UR	1405	11	52·27	3·75	13·16	13·10	0·17	4·65	7·93	2·66	1·80	0·51	0·57	324	36	54	134	105	30	39	673	40	305	26·6	576
DUP-34	UR	1420	11	52·85	3·80	13·12	13·01	0·19	4·36	8·31	2·70	1·11	0·56	1·05	326	35	61	182	112	29	47	882	38	309	28·5	682
DUP-33	UR	1435	11	52·35	3·79	12·96	13·25	0·16	4·50	8·38	2·68	1·35	0·59	1·06	358	36	56	182	114	26	20	829	41	312	28·0	609
DUP-12	PE	1385	11	51·08	3·72	13·13	14·04	0·17	4·65	8·23	2·56	1·83	0·59	0·94	379	40	42	177	125	25	41	706	38	311	30·4	608
DSM-27	SM	1390	11	52·64	3·76	12·91	13·09	0·15	4·50	8·48	2·23	1·72	0·52	1·21	337	n.a.	64	185	117	25	38	951	37	300	25·1	519
DSM-41	SM	1400	11	51·87	3·88	13·48	12·98	0·16	4·60	8·33	2·41	1·77	0·53	1·54	342	40	52	179	109	26	45	1050	44	307	27·0	670
DW-24	CO	1295	11	51·79	3·74	13·54	13·45	0·19	4·48	8·02	2·61	1·68	0·49	0·63	358	42	61	140	119	25	24	832	38	298	28·2	615
DSM-24	SM	1420	12	54·93	2·95	13·94	11·53	0·17	3·18	6·44	3·29	2·86	0·70	0·50	257	n.a.	25	72	137	26	72	552	48	391	38·4	776
DUP-32	UR	1450	13	51·35	4·21	12·87	13·83	0·19	4·40	7·68	2·67	2·22	0·58	0·10	398	45	65	160	121	27	44	737	41	326	32·9	673
DUP-31	UR	1465	13	51·23	4·15	12·96	14·02	0·18	4·53	8·67	2·62	1·08	0·55	1·10	371	38	65	196	119	26	21	884	42	328	32·3	684
DUP-11	PE	1375	13	51·20	4·13	12·98	14·16	0·17	4·50	8·99	2·30	1·00	0·58	1·94	364	39	51	201	109	29	21	840	40	328	33·2	628
DUP-13	PE	1420	13	51·38	4·16	12·71	13·94	0·19	4·35	8·37	3·13	1·21	0·56	1·26	341	40	49	170	114	32	39	892	46	326	32·3	753
DUP-29	UR	1505	14	51·44	4·20	12·91	13·57	0·19	4·29	8·24	3·25	1·31	0·60	0·96	361	39	59	191	110	22	46	930	40	339	35·7	718
DUP-28	UR	1520	14	51·42	4·20	12·92	13·49	0·17	4·42	8·33	2·98	1·47	0·59	0·72	362	36	49	185	110	30	41	875	38	330	32·3	715
DUP-20	PE	1490	14	51·23	4·33	13·13	13·50	0·17	4·39	8·07	2·72	1·88	0·58	0·33	375	45	59	192	129	20	43	833	42	344	34·5	732
DSM-22	SM	1445	14	51·34	4·23	13·14	13·40	0·16	4·35	7·87	2·89	2·03	0·59	0·83	393	38	54	188	125	27	47	707	39	336	32·9	615
DSM-21	SM	1450	14	51·49	4·21	13·17	13·43	0·17	4·32	7·27	3·05	2·29	0·60	1·76	379	39	55	190	130	24	59	608	41	339	33·1	727
DRR-12	RR	1355	14	51·13	4·20	13·27	13·92	0·17	4·42	8·32	2·55	1·44	0·58	0·72	n.a.	n.a.	48	196	125	27	19	938	41	334	32·8	n.a.
DSM-17a	SM	1540	15	51·83	4·16	13·07	13·39	0·16	4·12	7·62	2·91	2·11	0·61	0·91	370	39	51	169	114	24	43	789	40	343	31·5	707
DSM-17b	SM	1540	15	52·35	4·15	13·10	13·36	0·17	4·06	7·85	2·50	1·84	0·62	0·91	358	39	56	181	111	24	31	879	41	351	31·4	738
DRR-06	RR	1465	15	53·09	4·04	12·64	13·00	0·16	4·03	7·27	2·82	2·36	0·60	0·49	353	n.a.	45	165	133	25	41	662	39	346	32·4	691
ES-537	ES	404	15 ?	51·60	4·11	13·11	13·70	0·16	4·07	8·21	3·07	1·36	0·60	1·12	349	n.a.	57	n.a.	n.a.	n.a.	45	812	39	332	27·7	674
DSM-16	SM	1570	16	51·28	3·88	13·33	13·36	0·17	4·45	8·18	3·17	1·64	0·57	0·62	349	38	62	165	109	26	37	869	38	312	27·2	630
DSM-10	SM	1720	17	51·25	3·66	13·71	13·20	0·17	4·56	8·40	2·95	1·54	0·55	0·73	378	n.a.	54	152	122	26	58	826	36	306	28·5	592
DSM-05b	SM	1755	18	51·56	3·51	13·24	13·87	0·19	4·30	8·01	3·01	1·80	0·51	0·75	387	32	37	188	105	27	45	701	37	272	23·9	595
DSM-07	SM	1755	18	51·61	3·48	13·32	14·15	0·17	4·21	7·93	2·72	1·87	0·53	1·65	373	n.a.	34	200	124	26	47	690	39	282	24·5	570
DSM-09	SM	1755	18	51·43	3·49	13·32	14·05	0·17	4·37	8·04	2·94	1·71	0·50	0·86	407	37	39	165	113	27	41	372	36	259	23·7	563
DSM-04	SM	1765	19	59·78	2·01	14·06	9·20	0·14	2·05	4·11	3·84	4·12	0·70	0·87	119	n.a.	4	40	109	27	113	687	48	482	46·8	1137
DSM-08	SM	1765	19	59·96	2·03	13·86	9·38	0·15	1·92	4·11	3·89	4·01	0·69	0·88	122	17	3	44	114	27	109	600	50	499	47·9	1115

Sample	Road	Alt. (m)	Flow	SiO_2	TiO_2	Al_2O_3	Fe_2O_3	MnO	MgO	CaO	Na_2O	K_2O	P_2O_5	LOI	V	Co	Ni	Cu	Zn	Ga	Rb	Sr	Y	Zr	Nb	Ba
AV-1668	AV	−1151	b/h	51·77	3·58	13·28	13·71	0·19	3·90	7·80	3·13	1·93	0·71	n.a.	309	31	22	100	108	25	49	829	42	276	29·7	657
GO-1053	GO	−137	b/h	50·41	3·91	13·32	14·36	0·17	4·61	8·20	2·78	1·74	0·50	n.a.	342	42	45	132	109	27	36	813	37	277	26·7	571
RO-1185	RO	−437	b/h	51·83	3·47	13·40	13·55	0·19	3·92	7·55	3·29	2·06	0·75	n.a.	332	n.a.	24	n.a.	n.a.	n.a.	50	770	39	289	26·7	682
DAB-01	AB	1200	dyke	51·40	3·67	13·52	13·02	0·17	4·63	7·48	3·53	2·05	0·51	1·36	345	n.a.	55	152	125	26	51	811	39	309	28·2	661
DSM-26	SM	1435	dyke	52·10	3·41	13·89	12·18	0·17	4·39	8·39	2·77	1·87	0·46	1·40	345	n.a.	65	182	102	23	39	783	36	295	25·2	579
DW-22	Aiure	—	dyke	50·85	3·57	13·14	14·50	0·19	4·47	8·04	2·94	1·78	0·53	0·39	387	34	45	138	119	25	55	588	38	279	27·5	630
DRG-6	Aiure	—	dyke	50·55	3·66	13·19	14·84	0·19	4·50	7·67	2·90	1·97	0·53	0·38	n.a.	n.a.	39	139	123	25	55	577	40	296	27·7	n.a.
ST93-1	FD	—	dyke	51·43	4·13	13·28	13·67	0·17	4·15	8·09	2·55	1·92	0·61	0·46	360	39	51	190	128	26	40	786	42	352	31·5	709
ST93-2	FD	—	dyke	51·68	4·03	13·33	13·61	0·17	4·12	7·76	2·70	1·99	0·62	0·45	345	38	53	195	120	28	54	816	42	352	31·6	714
ST93-3	FD	—	dyke	51·86	3·68	13·38	12·88	0·16	4·66	7·43	2·79	1·66	0·50	1·11	346	39	68	164	127	23	48	620	40	318	28·6	540
ST93-4	FD	—	dyke	52·16	3·66	13·34	12·96	0·16	4·61	8·35	2·65	1·62	0·49	0·03	350	39	69	170	128	24	31	746	40	320	27·9	597
ST93-5	FD	—	dyke	54·82	2·63	13·08	13·44	0·20	2·69	6·53	3·07	2·50	1·05	1·33	127	25	7	38	156	27	58	519	61	433	36·1	721
Low-Ti Palmas rhyolites																										
DGB-61	GB	1430	unit F	69·21	0·88	12·73	5·66	0·10	1·22	2·53	2·47	4·95	0·26	0·72	n.a.	n.a.	10	53	72	19	188	113	44	256	22	n.a.
DGB-59	GB	1475	unit F	67·44	0·99	13·29	6·39	0·11	1·37	3·76	3·50	2·88	0·27	2·28	42	n.a.	5	77	78	19	157	156	42	255	22	573
DGB-58	GB	1495	unit F	67·52	0·98	13·29	6·37	0·11	1·33	3·64	3·58	2·92	0·26	2·21	n.a.	n.a.	8	72	81	18	171	164	42	265	21	n.a.
ES-312	ES	629	unit F	67·15	0·98	14·02	5·86	0·12	1·83	3·76	2·69	3·27	0·31	2·39	n.a.	n.a.	8	54	93	22	75	160	46	278	23	n.a.
ES-216a	ES	725	unit G	67·80	1·08	12·90	6·43	0·11	0·81	3·01	3·26	4·28	0·32	0·47	n.a.	n.a.	9	96	77	17	170	145	47	280	23	n.a.
ES-216b	ES	725	unit G	69·65	1·00	12·12	6·03	0·10	0·86	2·99	3·20	3·75	0·31	0·47	n.a.	n.a.	8	96	68	18	147	135	44	253	20	n.a.
ES-150	ES	791	unit G	67·83	1·07	12·86	6·36	0·12	1·04	3·19	3·48	3·75	0·31	0·48	n.a.	n.a.	8	98	72	14	160	148	46	269	21	n.a.
ES-123	ES	818	unit G	68·33	1·03	12·72	6·08	0·09	1·11	3·29	3·34	3·70	0·31	0·69	n.a.	n.a.	8	86	76	19	166	149	47	269	21	n.a.
ES-105	ES	836	unit G	67·80	1·06	12·83	6·42	0·11	1·10	3·30	3·41	3·67	0·32	0·48	n.a.	n.a.	9	110	76	20	158	147	46	265	21	n.a.
ES-087	ES	854	unit G	67·61	1·05	12·77	6·39	0·12	1·17	3·18	3·19	4·22	0·31	0·52	n.a.	n.a.	10	104	82	19	175	131	45	260	20	n.a.

X-ray fluorescence major and trace element data. Major element data are normalized to 100% on a volatile-free basis, with total iron as Fe_2O_3(t). Analytical details, plus estimates of analytical uncertainties, given by Peate & Hawkesworth (1996). n.a., not analysed. Alt., Altitude measured using an altimeter in conjunction with existing trigonometric survey points to an estimated precision of $\pm$5 m (all altitudes in table and text are in metres above sea level). LOI, loss on ignition. Road profile locations: PE, Perico (28·14°S, 49·66°W); UR, Urubici (28·08°S, 49·62°W); SM, São Jose–Morro da Igreja (28·12°S, 49·46°W); AB, Aguas Brancas (27·90°S, 49·58°W); CO, Corvo Branco (28·07°S, 49·30°W); RR, Rio Rufino (27·91°S, 49·89°W); GB, Guarta–Bom Jardim da Serra (28·36°S, 49·60°W); Aiure (28·35°S, 49·32°W). Borehole (b/h) locations: AV, Agua de Valenca (23·094°S, 51·913°W); RO, Roncador (24·609°S, 52·247°W); GO, Galvão (26·383°S, 52·710°W); ES, Esmeralda (28·093°S, 51·154°W). FD, Florianopolis dyke swarm (samples collected from Ponta do Retiro on the east coast of Santa Catarina island, ~10 km southeast of Florianopolis). For definition of unit F and unit G rhyolites. Unit F rhyolites belong to the Caxias do Sul subgroup of the Palmas rhyolites, and unit G rhyolites belong to the Anita Garibaldi subgroup of the Palmas rhyolites (Garland *et al.*, 1996) [See Milner *et al.* (1995*a*)].

Table 2: Additional trace element data for Urubici magma type samples

Sample	Unit	Flow	Sc	Cs	La	Ce	Nd	Sm	Eu	Tb	Yb	Lu	Hf	Ta	Pb	Th	U
DUP-02	B	3	26·8	0·5	43·2	93·8	50·8	11·2	3·58	1·59	3·18	0·50	8·12	1·98	n.a.	4·71	1·15
DSM-36	A	6	n.a.	n.a.	n.a.	n.a.	n.a.	n.a.	n.a.	n.a.	n.a.	n.a.	n.a.	n.a.	7·51	n.a.	n.a.
DSM-35	A	7	34·0	0·4	37·8	80·4	49·3	10·5	3·19	1·44	2·95	0·46	7·08	1·71	5·58	4·16	1·77
DSM-34	A	8	23·8	1·2	39·2	79·3	43·7	9·26	2·91	1·23	2·33	0·38	6·67	1·70	6·81	4·49	1·04
DSM-30	C	10	26·0	n.d.	37·2	83·3	46·3	9·81	3·38	1·47	2·77	0·44	7·55	1·75	5·67	3·77	0·98
DUP-37	C	10	20·1	1·3	37·1	79·4	45·9	10·4	3·21	1·40	2·71	0·42	7·18	1·68	n.a.	3·62	1·27
DUP-35	C	11	28·9	0·3	42·5	90·4	54·3	11·6	3·53	1·54	2·99	0·44	7·97	1·92	n.a.	4·25	1·34
DSM-27	C	11	25·0	1·2	38·0	83·2	47·7	10·2	3·43	1·51	2·76	0·41	7·61	1·78	n.a.	3·86	0·76
DSM-24	E	12	19·7	0·6	60·5	126	63·5	12·6	4·03	1·72	3·66	0·56	9·32	2·53	9·48	7·39	2·01
DUP-32	D	13	33·0	0·5	49·0	108	60·6	12·8	3·98	1·83	3·29	0·49	8·70	2·30	n.a.	5·20	1·36
DSM-17b	D	15	24·6	1·1	48·6	110	62·4	13·0	4·02	1·74	3·12	0·49	9·30	2·35	n.a.	5·11	1·86
DSM-10	E	17	25·2	1·7	42·0	92·7	51·6	10·6	3·53	1·44	2·76	0·42	7·78	2·03	6·49	4·78	1·13
DSM-05b	E	18	27·0	0·6	39·8	87·5	49·0	10·3	3·41	1·47	3·12	0·47	7·30	1·89	7·31	5·02	1·08
DSM-07	E	18	27·0	0·6	40·7	88·5	50·8	10·2	3·37	1·45	3·11	0·48	7·44	1·91	7·35	5·20	1·37
DSM-04	E	19	13·8	1·8	79·6	173	82·6	15·3	4·42	1·85	3·63	0·55	12·4	3·32	14·2	12·1	3·00
DSM-08	E	19	14·1	1·8	81·1	180	85·6	15·9	4·65	2·00	3·92	0·56	12·3	3·20	n.a.	12·8	2·71
DSM-26	—	dyke	24·5	n.d.	39·9	93·1	51·7	10·8	3·56	1·59	2·83	0·44	7·59	1·90	n.a.	4·47	1·40
WS observed	—	—	—	1·03	25·4	57·8	33·5	7·20	2·29	1·14	2·56	0·41	4·95	1·30	n.a.	3·08	0·96
(n = 7) 1σ	—	—	—	0·04	0·8	0·7	1·0	0·24	0·04	0·05	0·08	0·01	0·09	0·02	n.a.	0·06	0·15
WS expected	—	—	—	1·03	25·5	57·5	32·9	7·27	2·25	1·09	2·54	0·39	4·93	1·26	n.a.	3·05	0·90

All data by instrumental neutron activation analysis at the Open University, following the procedure of Potts *et al.* (1985), except for Pb, which was analysed by isotope dilution on a VG54E mass spectrometer at the Open University. Precision and accuracy of the neutron activation technique can be estimated from the standard deviations from repeat analyses of WS (in-house standard) and by comparing the observed values for WS with expected values from Potts *et al.* (1985). Isotope dilution measurement of BHVO-1 gave 2·04 ppm Pb. n.a., not analysed; n.d., not detected; *n*, number of analyses.

LOCAL FLOW STRATIGRAPHY

Rationale of approach to flow correlation

Exposure is seldom continuous and mainly consists of scattered isolated outcrops with dense vegetation obscuring the areas between. This prevents visual correlation of individual flows between profiles. Physical characteristics of the lavas such as jointing habit, flow thickness and morphology, and petrographic textures, are of little value in flow correlation. Such features are often not unique to an individual flow and they can vary markedly within a single flow over a few kilometres, because they are controlled primarily by lateral variations in the local cooling conditions, palaeotopography, and by distance from the vent source. Most Paraná basalts are subaphyric with broadly similar phenocryst assemblages (Comin-Chiaramonti *et al.*, 1988): even the high-Ti/Y Urubici and low-Ti/Y Gramado basalts cannot be distinguished petrographically. The only petrographically distinct Urubici flow is the dacite flow (DSM-04,08) which has 30% phenocrysts, but it is found in one profile (the uppermost unit in the SM profile).

Instead, flows are distinguished and correlated from small variations in TiO_2 and MgO (Fig. 6) and from their relative stratigraphic position in each profile. TiO_2 is used because of its relative immobility during post-eruption alteration (e.g. Wood *et al.*, 1976) and because Urubici samples have a wide range of TiO_2 contents for a given MgO content (Fig. 6). We recognize a minimum of 19 Urubici flows in the São Joaquim area. Their correlation between profiles is shown in Fig. 7. A thin (<5 m) horizon of aeolian sandstone separates flows 6 and 7 and indicates a persistence of the arid desert climate that typifies the sediments of the underlying Botucatu Formation. Flow contacts are recognized in the field by the presence of a vesicular aa-type flow-top and a sharp transition to the more massive base of the subsequent flow. It is often difficult to determine whether these are true inter-flow contacts or represent an internal contact within a compound-type flow, given the discontinuous nature of the exposure. Although flows 9 and 10 are compositionally very similar, they are clearly two distinct flows because in the UR profile they are separated by a Gramado flow (Fig. 7). Thus, several of the flows

Table 3: Radiogenic isotope data for Urubici magma type samples, and selected low-Ti/Y Palmas rhyolites

Sample	Unit	Flow	$^{87}Sr/^{86}Sr$ measured	$^{87}Sr/^{86}Sr$ initial	ε_{Sr} initial	$^{143}Nd/^{144}Nd$ measured	$^{143}Nd/^{144}Nd$ initial	ε_{Nd} initial	$^{206}Pb/^{204}Pb$ measured	$^{207}Pb/^{204}Pb$ measured	$^{208}Pb/^{204}Pb$ measured
DGB-09	A	1	0·70607	0·70557	14·9	n.a.	n.a.	n.a.	17·591	15·498	38·156
DUP-02	B	3	0·70544	0·70529	10·6	0·512449	0·51234	−2·7	17·603	15·494	38·140
DUP-04	A	5	0·70587	0·70561	15·1	0·512360	0·51225	−4·3	17·727	15·514	38·231
DSM-36	A	6	0·70628	0·70590	19·2	0·512276	0·51217	−5·9	17·543	15·515	38·201
DSM-35	A	7	0·70574	0·70550	13·6	0·512380	0·51227	−3·9	17·553	15·488	38·186
DUP-42	A	8	0·70572	0·70541	12·3	0·512395	0·51229	−3·6	17·538	15·464	38·032
DSM-34	A	8	0·70592	0·70572	16·8	0·512383	0·51227	−3·9	17·704	15·535	38·334
DSM-30	C	10	0·70547	0·70518	9·1	0·512403	0·51229	−3·5	17·517	15·486	38·039
DUP-37	C	10	0·70565	0·70531	10·8	0·512438	0·51232	−3·0	17·519	15·477	38·033
DUP-35	C	11	0·70527	0·70506	7·4	0·512407	0·51230	−3·4	17·464	15·458	38·026
DSM-27	C	11	0·70523	0·70502	6·7	0·512455	0·51235	−2·5	17·541	15·490	38·065
DSM-24	E	12	0·70644	0·70575	17·1	0·512328	0·51223	−4·8	18·040	15·543	38·367
DUP-32	D	13	0·70520	0·70488	4·8	0·512452	0·51234	−2·5	17·776	15·505	38·227
DSM-22	D	14	0·70519	0·70483	4·1	0·512469	0·51236	−2·2	17·788	15·496	38·131
DRR-06	D	15	0·70531	0·70499	6·3	0·512459	0·51235	−2·4	17·728	15·501	38·141
DSM-17b	D	15	0·70515	0·70496	5·9	0·512482	0·51237	−1·9	17·749	15·505	38·148
DSM-10	E	17	0·70547	0·70509	7·8	0·512405	0·51230	−3·4	17·960	15·556	38·367
DSM-05b	E	18	0·70593	0·70558	14·8	0·512424	0·51232	−3·1	18·138	15·573	38·452
DSM-07	E	18	0·70591	0·70554	14·1	0·512429	0·51233	−2·9	18·131	15·558	38·406
DSM-04	E	19	0·70746	0·70657	28·8	0·512360	0·51226	−4·1	18·253	15·584	38·612
DSM-08	E	19	0·70743	0·70645	27·1	0·512357	0·51226	−4·1	18·202	15·565	38·535
DSM-26	—	dyke	0·70538	0·70511	8·0	0·512455	0·51235	−2·4	17·668	15·504	38·210
DAB-03	—	dyke	0·70584	0·70543	12·6	0·512467	0·51236	−2·2	n.a.	n.a.	n.a.
DGB-59	unit F rhyolite		0.72335	0·71793	190·0	0·512233	0·51213	−6·8	n.a.	n.a.	n.a.
DGB-61	unit F rhyolite		0.72879	0·71987	217·5	0·512166	0·51206	−8·1	n.a.	n.a.	n.a.

All data measured on a Finnigan MAT261 mass spectrometer at the Open University. Sr and Nd isotopic fractionation corrections are $^{86}Sr/^{88}Sr = 0{\cdot}1194$ and $^{144}Nd/^{146}Nd = 0{\cdot}7219$. NBS 987 Sr standard gave a mean value of $0{\cdot}710228 \pm 17$ and Johnson & Mathey (J&M) Nd standard gave a mean value of $0{\cdot}511864 \pm 14$ during this study. Data presented relative to NBS 987 Sr 0·71025 and J&M Nd 0·51185 (equivalent to BCR-1 0·51265). Initial ratios calculated at 132 Ma. Sm/Nd is constant ($0{\cdot}212 \pm 0{\cdot}006$) for the basaltic samples ($SiO_2 < 54$ wt %), and this value was used in the calculation of initial Nd isotope data if Sm and Nd were not measured directly. Similarly, an average Sm/Nd value ($0{\cdot}209 \pm 0{\cdot}006$: Hawkesworth *et al.*, 1988; Garland *et al.*, 1995) was assumed for the rhyolite data. Measured Pb isotope ratios corrected for an average 0·8‰ per a.m.u. fractionation relative to recommended values for NBS 981 Pb standard (Todt *et al.*, 1996). Reproducibility of Pb standard data was ~0·07% for $^{206}Pb/^{204}Pb$ and $^{207}Pb/^{204}Pb$, and ~0·11% for $^{208}Pb/^{204}Pb$. Within-run errors (2 SE) on Sr–Nd–Pb sample data are less than or equal to the external uncertainties (2 SD) on the standards. Total procedure blanks were <2 ng for Sr and Nd, and <1 ng for Pb. n.a., not analysed.

recognized might represent multiple eruptions of compositionally similar magma, and this could account for some of the compositional scatter within groups of samples assigned to the same flow (Fig. 6).

Implications of flow correlations

Most flows are found in more than one sampled profile, but exceptions include the upper four flows at the SM profile (flows 16–19), which lie at a higher stratigraphic level than flows in the surrounding profiles, where the higher-level lavas have probably been removed by erosion. The andesitic flow 12 is found only at the SM profile, although from stratigraphic considerations it should also have been found at the RR, UR and PE profiles, and this suggests that it has a relatively restricted spatial extent. Flows 3, 4 and 5, found at the base of the PE profile below a NW–SE trending fault, are correlated with the uppermost flows at the GB profile to the south. These flows are not found in the neighbouring SM and UR profiles, although flows 4 and 5 are found in the AB profile, which has a lower elevation than the surrounding profiles and has been strongly affected by faulting (Figs

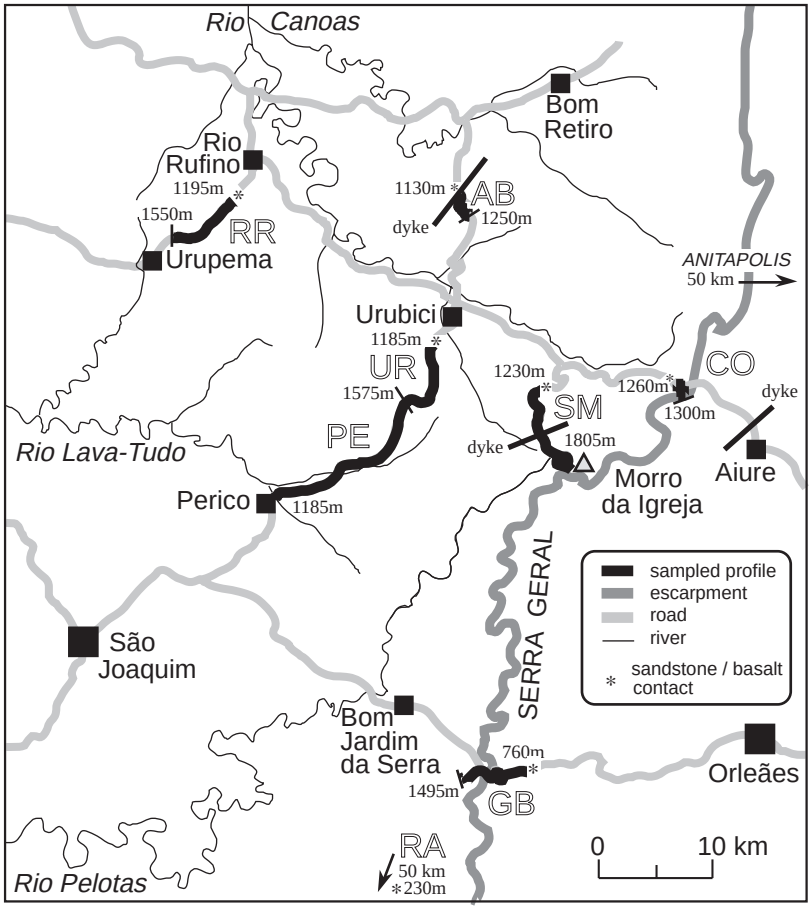

Fig. 4. Map of São Joaquim study area, showing the location of the sampled road profiles and the local physiography. The Serra Geral escarpment (dark grey line) marks an abrupt change in elevation between the coastal plain in the east and the high lava plateau in the west. The altitude of the top and base of each road profile are marked in metres above sea level. The basal contact of the lavas with the Botucatu Formation sandstones, if encountered, is indicated by an asterisk.

4 and 7). Flows 1 and 2 are found only near the base of the GB profile. The single Urubici flow found at the RA profile to the south (Bellieni *et al.*, 1984) cannot be correlated with any flows found in the GB profile. At profiles SM and UR, flow 9 overlies three lower Urubici flows (flows 6, 7 and 8), whereas it is the lowest Urubici flow found at the RR profile and it lies directly on the sediments at the CO profile. Thus, the lavas in the São Joaquim region successively overstep the underlying sediments to the north-east, consistent with a pre-eruption topographic relief of at least 400 m (Fig. 7). Palaeotopography was also an important control on flow thickness; for example, the basal Gramado-type flow at the GB profile is up to 60 m thick and fills in an existing valley cut into the underlying sedimentary rocks (de Oliveira, 1956). The thickness of individual flows (average ~20 m) varies non-systematically across the area although significant uncertainties arise in the estimates for many flows because of the lateral distance between exposures: the road profiles covered distances of 5–15 km to sample vertical lava profiles of 400–750 m.

On a regional scale, the elevation of the base of the lava pile rises significantly in a direction parallel to the coast northwards along the Serra Geral escarpment (Peate *et al.*, 1992) from 230 m at the RA profile to 1260 m at the CO profile, 100 km to the north (Fig. 4). It is not clear whether this feature is, to a large extent, an original topographic feature formed before the Paraná magmatism, or the result of subsequent differential uplift. Gallagher *et al.* (1994) argued from fission-track data for large-scale (i.e. several kilometres) uplift of the whole Serra Geral escarpment, although pre-existing topography was clearly important on a local scale in controlling the emplacement of lavas in the São Joaquim region. The borehole sample ES-537 (elevation 404 m) is compositionally identical to flow 15 (average elevation ~1500 m) (Fig. 6a). If they are the same flow, then this implies that the São Joaquim region has been uplifted

by ~1 km relative to the ES borehole, which is located ~150 km to the west (Fig. 2). Further evidence for significant post-magmatism differential uplift comes from the correlation of compositionally distinct rhyolite units. The rhyolite flows capping the GB profile (1430–1500 m: Fig. 7) are compositionally similar to the unit F rhyolites of Milner *et al.* (1995*a*), which are found about 500 m lower (950–1000 m) in the RA profile, and the difference in elevation of the base of the lava pile between the two profiles is of a similar magnitude (~500 m: RA 230 m; GB 760 m) (S. Milner, personal comunication, 1997). In the ES borehole (Fig. 2), rhyolites found at an elevation of ~630 m are similar to the unit F flows found ~350 m higher at the RA profile, and rhyolites from the upper part of the borehole (720–850 m) are compositionally similar to the unit G rhyolites of Milner *et al.* (1995*a*) found at 1080–1160 m in the RA profile (compositional data for the rhyolites from the GB profile and the ES borehole are in Table 1). Thus, post-magmatic uplift on the coastal Serra Geral escarpment, relative to the position of the inland ES borehole, is greatest at the GB profile (~1 km) and less at the RA profile to the south (~0·4 km).

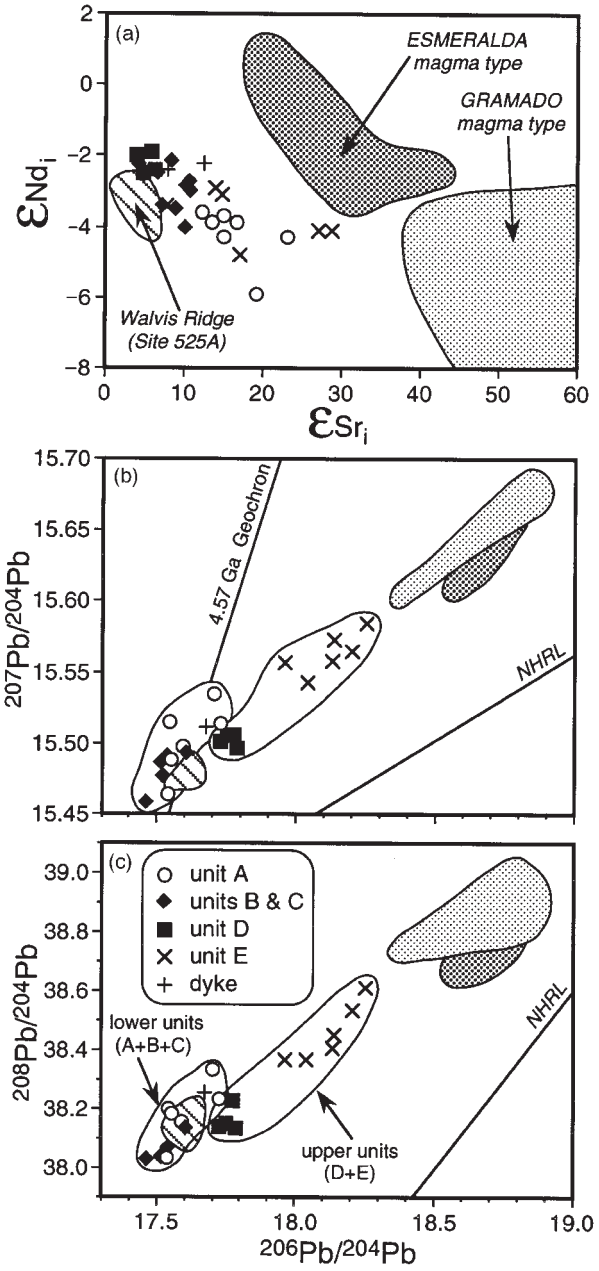

Fig. 5. Radiogenic isotope composition of the Urubici magma type, and comparison with the low-Ti/Y Gramado and Esmeralda magma types (Hawkesworth *et al.*, 1988; Peate & Hawkesworth, 1996). Units A–E are groups of compositionally similar, stratigraphically adjacent, Urubici flows, and are a convenient means to simplify later discussions (see text). (a) ε_{Nd_i} vs ε_{Sr_i}; (b) $^{207}Pb/^{204}Pb$ vs $^{206}Pb/^{204}Pb$, (c) $^{208}Pb/^{204}Pb$ vs $^{206}Pb/^{204}Pb$. The isotopic similarity of the unit C and D Urubici samples with the DSDP Site 525A Walvis Ridge samples (Richardson *et al.*, 1982) is striking. NHRL, Northern Hemisphere Reference Line (Hart, 1984). No Urubici samples in this study have the very low $^{206}Pb/^{204}Pb$ values (<17·4) found by Hawkesworth *et al.* (1986). The cause of the discrepancy is uncertain, although the data of Hawkesworth *et al.* (1986) were determined in a different laboratory (Oxford). Two otherwise compositionally very similar samples from the same flow in the GB profile have very different $^{206}Pb/^{204}Pb$ (DGB-09 17·59, Table 3; GB13af 17·06, Hawkesworth *et al.*, 1986). Post-eruption alteration can produce variable U/Pb within a single flow. However, the measured difference in $^{206}Pb/^{204}Pb$ of 0·5 would require a large difference in μ of ~25 and, although U and Pb contents were not determined for DGB-09, all the Urubici samples for which U and Pb data exist have relatively low μ ≪20.

SHALLOW-LEVEL EVOLUTION OF THE URUBICI MAGMA TYPE

Stratigraphic variations

The evolution of the Urubici magmas cannot be described by a single liquid line of descent from a homogeneous parental magma. This is evident both from the range in isotopic composition and from the fact that samples with, for example, 4·5 wt % MgO have a wide range in TiO_2 from 3·4 to 4·3 wt % (Fig. 6). Consideration of sequential variations in flow composition (Fig. 8) might help to unravel the nature of the processes controlling the evolution of the magmas. The Urubici flows are grouped into five units (A–E) to simplify subsequent discussions and to emphasize some of the general stratigraphic variations. The units have similar compositions based on groupings from Fig. 6 (MgO vs TiO_2) and isotope composition, and in general comprise stratigraphically adjacent flows (Fig. 8). A distinction is made between the

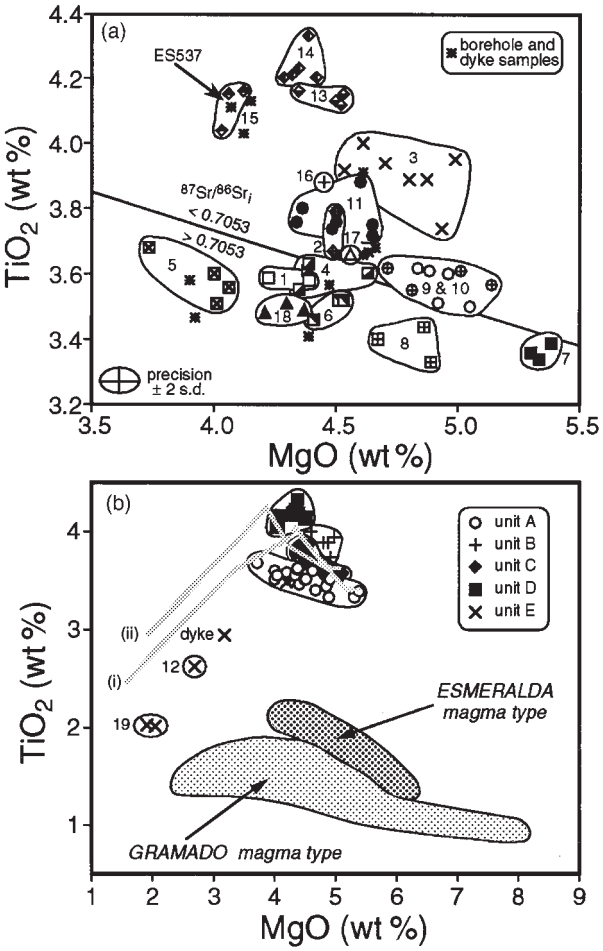

Fig. 6. (a) Nineteen compositionally distinct Urubici flows are recognized within the São Joaquim sequences from small differences in MgO and TiO_2 contents and their stratigraphical position (Fig. 7). All samples from a particular flow have the same symbol. The line separates samples with $^{87}Sr/^{86}Sr_i$ > or < 0·7053. (b) This panel shows data for the high-SiO_2 (>54 wt %) samples (flows 12 and 19, coastal dyke ST93-5), and also the clear compositional gap between the Urubici magmas and the low-Ti/Y Gramado and Esmeralda magmas sampled from the same road profiles (Peate & Hawkesworth, 1996). The grey lines are low-pressure (1 kbar) fractionation paths modelled for two parent magmas [(i) flow 7, (ii) flow 9/10] using the MELTS program (Ghiorso & Sack, 1995) with $f(O_2)$ set at the QFM buffer.

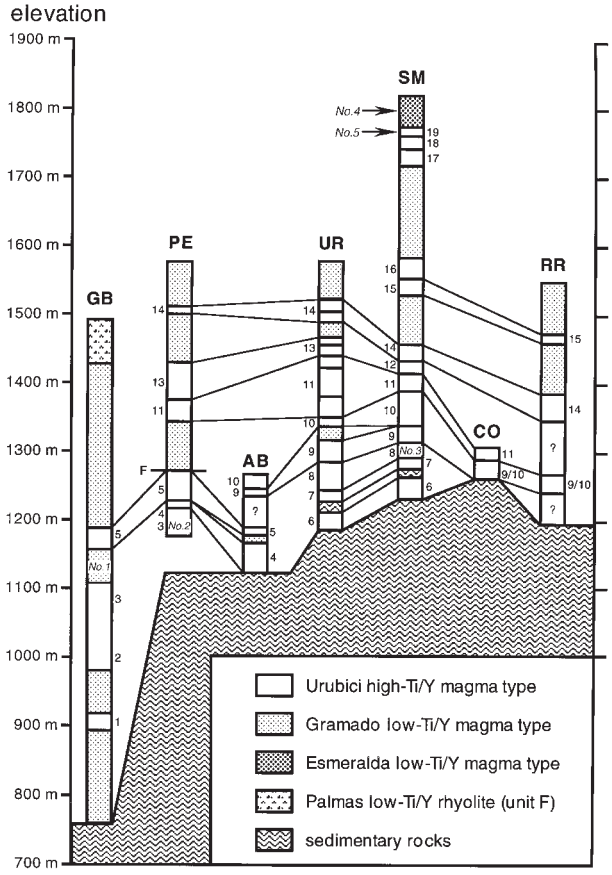

Fig. 7. Local correlation of Urubici flows from Fig. 6 between the São Joaquim road profiles, which highlights the local importance of pre-existing topographic relief in controlling the emplacement of lava flows. $^{40}Ar/^{39}Ar$-dated samples: No. 1, GB40c, 132·4 ± 0·7 Ma; No. 2, DUP-01, 130·2 ± 1·1 Ma; No. 3, DSM-34, 132·3 ± 0·8 Ma; No. 4, DSM-05a, 129·4 ± 1·3 Ma (No. 1: Renne *et al.*, 1992; Nos 2, 3, 4: Turner *et al.*, 1994). No. 5, DSM-08, 132 ± 5 Ma apatite fission-track age (Gallagher *et al.*, 1994).

lower units (A, B, C) and the upper units (D, E) from Pb isotope data (Fig. 5). Unit A flows (1, 4–8) have the lowest TiO_2 contents and high $^{87}Sr/^{86}Sr_i$ >0·7053. Unit B flows (2, 3) and unit C flows (9–11) have higher TiO_2 and low $^{87}Sr/^{86}Sr_i$ <0·7053, whereas the unit D flows (13–15) have very high TiO_2 (>4·0 wt %) and low $^{87}Sr/^{86}Sr_i$ <0·7050. Unit E comprises the two evolved flows (12 and 19) and the uppermost basaltic flows (16–18). These flows have high $^{87}Sr/^{86}Sr_i$ >0·7053, but are distinguished from the unit A flows by their high $^{206}Pb/^{204}Pb$ (17·9–18·3).

Major element systematics and fractional crystallization models

Urubici samples plot on the 1 atm cotectic (ol + pl + cpx + liq) in the CIPW normative Di–Ol–Hy–Qz/Ne diagram of Thompson *et al.* (1983) (Peate, 1990), which indicates that they equilibrated and crystallized at low pressures in near-surface magma reservoirs. The major element characteristics of the Urubici magmas are consistent with fractionation of an olivine–clinopyroxene–plagioclase assemblage (Bellieni *et al.*, 1984). This fractionation leads to near-constant SiO_2 and Al_2O_3, a decrease of CaO, and the development of the typical tholeiitic differentiation trend of Fe_2O_3 and TiO_2 enrichment, as MgO decreases (Cox, 1980). This is best shown by the low $^{87}Sr/^{86}Sr_i$ units (B, C, D). The plausibility of generating this trend by fractional crystallization can be tested with least-squares major element mixing

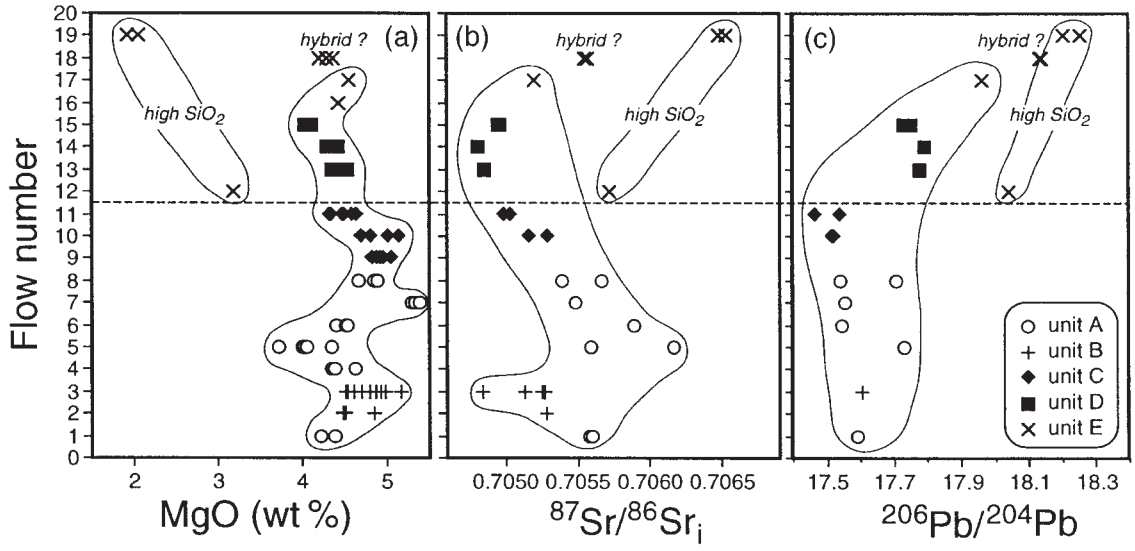

Fig. 8. Stratigraphical variations in Urubici flow compositions in the São Joaquim area. Flow number vs (a) MgO, (b) $^{87}Sr/^{86}Sr_i$, (c) $^{206}Pb/^{204}Pb$. Dashed line indicates approximate division into lower units (A–C) and upper units (D and E). MgO and $^{87}Sr/^{86}Sr_i$ data on Urubici samples from GB profile from Mantovani *et al.* (1985) are also plotted.

models. A good model fit (Peate, 1990) is obtained for the composition of the flow with the highest TiO_2 (flow 13: MgO 4·4 wt %, TiO_2 4·2 wt %) by 15% crystallization of olivine–plagioclase–clinopyroxene in the proportions 15/47/38, starting from the most mafic flow (flow 7: MgO 5·4 wt %, TiO_2 3·3 wt %). This calculated crystallizing assemblage is similar to the typical tholeiitic extract of Cox (1980), namely, 15/50/35. These trends can be approximately reproduced by low-pressure (1 kbar) fractionation using the MELTS program of Ghiorso & Sack (1995), taking either flow 7 or flow 9/10 as the initial composition and setting $f(O_2)$ conditions at the QFM buffer (Fig. 6). Magnetite joins the fractionating phases for samples with MgO <4·2 wt %, producing a strong decrease in Fe_2O_3 and TiO_2 (Fig. 6), and contributing to the rapid increase in SiO_2. Constant P_2O_5 contents in the andesite and dacite flows reflect crystallization of minor amounts of apatite, which can be found as small euhedral crystals in the porphyritic dacite flow 19.

The high $^{87}Sr/^{86}Sr_i$ (>0·7053) unit A flows are anomalous and define a shallow trend in Fig. 6, with only a slight increase in TiO_2 as MgO decreases. This trend, from flow 7 (MgO 5·4 wt %, TiO_2 3·3 wt %) to flow 4 (MgO 4·0 wt %, TiO_2 3·6 wt %) can be modelled by 15% crystallization of an olivine–plagioclase–clinopyroxene–magnetite assemblage in the proportions 10/33/53/5. This extract involves an unrealistically high proportion of the Ti-rich phases augite and magnetite, which are required so that the bulk distribution coefficient for Ti is close to one. Successive flows within unit A do not define a simple temporal trend of decreasing MgO that might indicate progressive fractionation. Instead, it is more likely that the shallow trend represents mixing between relatively evolved and relatively primitive liquids. Within unit A, the flows with lower MgO tend to have higher SiO_2 and $^{87}Sr/^{86}Sr_i$, which suggests that the more evolved end-member suffered more crustal interaction.

Crustal assimilation

Crustal assimilation should have a limited effect on Urubici magmas because of their high incompatible trace element contents. Crustal rocks generally have high $\delta^{18}O$ relative to the mantle average value of +5·5‰, and so oxygen isotope data offer one means by which to assess the extent, if any, of crustal input to these mantle-derived magmas. The sparse $\delta^{18}O$ data obtained on whole-rock Urubici samples are primarily controlled by water–rock interactions (Iacumin *et al.*, 1991). Whole-rock samples of the equivalent Khumib magma type in the Etendeka have high $\delta^{18}O$ (+8 to +11‰), whereas clinopyroxene mineral separates give lower $\delta^{18}O$ (+5·9 to +6·0‰) only slightly elevated above the values expected for clinopyroxenes in equilibrium with uncontaminated mantle-derived basalts (Harris *et al.*, 1989).

Correlations exist between certain incompatible trace element ratios and radiogenic isotope ratios that suggest that some crustal assimilation did take place, although to a much lesser extent than in the low-Ti/Y Gramado magma type (Peate & Hawkesworth, 1996). There is a positive correlation between Th/Ta and $^{87}Sr/^{86}Sr_i$ (Fig. 9a) and a negative correlation between La/Ta and ε_{Nd_i} (Fig. 9b), implying addition of material with high

$^{87}Sr/^{86}Sr_i$, low ε_{Nd} and a significant negative Ta–Nb anomaly, all features typical of continental crust. The strong crustal influence seen in the local low-Ti/Y magmas (Gramado basalts; Peate & Hawkesworth, 1996: Palmas rhyolites; Garland *et al.*, 1995) means that mixing of these magmas with an Urubici magma could also mimic many of the compositional effects of crustal assimilation. Th/Ta and $^{87}Sr/^{86}Sr_i$ correlate with increasing SiO_2 going from the basalts to the andesite and dacite flows, but data for the evolved flows do not lie on a mixing line between data fields for the basalts and the low-Ti/Y magmas. This is apparent from Fig. 9c, where the andesite and dacite data plot at higher Zr contents than values for the Urubici basalts and the low-Ti/Y Gramado and Palmas magmas. Instead, these rare, high-SiO_2 (>54 wt %) flows probably result from a localized style of contamination where the amount of assimilation is linked thermally to the extent of crystallization [e.g. AFC (assimilation–fractional crystallization) model of DePaolo (1981)]. The basaltic flow 18, found near the top of the SM profile, is the only Urubici flow that has some compositional features that might indicate that it is a hybrid flow. Samples of this flow plot beneath the main trend on Fig. 9c and have the lowest $(Tb/Yb)_N$ ~2·1 of the Urubici basalts [where subscript N denotes chondrite-normalized using the values of Sun & McDonough (1989)]. It is possible to explain these features, as well as the Sr–Nd–Pb isotope composition, by mixing ~30% of an average low-Ti/Y Gramado magma with a unit D Urubici magma. It is notable though, that the three samples of this flow (DSM-05b, -07, -09), taken over a lateral distance of 1 km, indicate a rather homogeneous composition.

The Urubici basalts show poor correlations between isotope composition and indices of fractionation such as MgO, except for the unit A flows as mentioned in the previous section. On a broad scale, there is a general decrease in $^{87}Sr/^{86}Sr_i$ with increasing stratigraphic height for the basalts (Fig. 8). This suggests that the extent of contamination was decreasing with time, perhaps as a result of the more readily mobilized crustal material having been scavenged from the conduit walls by the earlier flows.

There is a general positive correlation between $^{87}Sr/^{86}Sr_i$ and $^{206}Pb/^{204}Pb$ for the Urubici data (Fig. 10). In detail, the lower units (A–C) and the upper units (D and E) form two parallel trends, and each is interpreted as reflecting assimilation of crustal material with high $^{87}Sr/^{86}Sr$ and $^{206}Pb/^{204}Pb$ but starting from two compositionally distinct end-members represented by units C and D, respectively. Two trends are also apparent from the Pb–Pb isotope diagrams (Fig. 5), where the lower and upper units form two en-echelon trends, with increased contamination leading to higher Δ7/4. The lower and

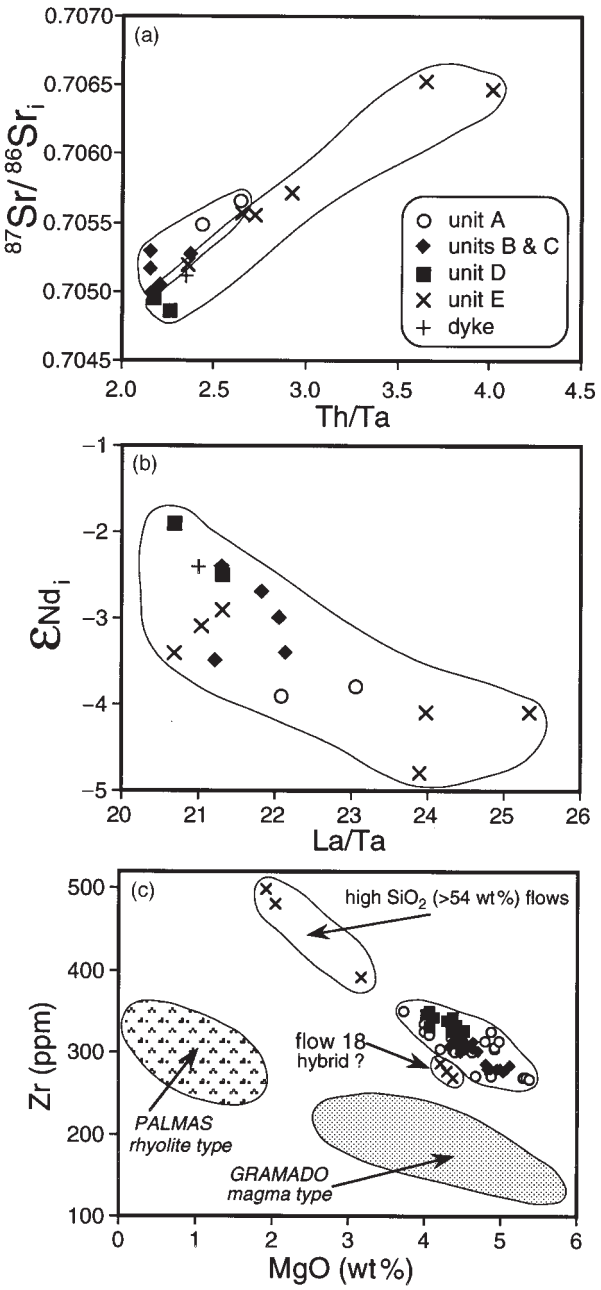

Fig. 9. Diagrams illustrating the effects of crustal assimilation and mixing on some Urubici flows. (a) $^{87}Sr/^{86}Sr_i$ vs Th/Ta, (b) ε_{Nd_i} vs La/Ta. Data from Mantovani *et al.* (1985) are not included in (a) or (b) because the Ta data are ~0·5 ppm higher than the data of this study. (c) Zr vs MgO. The high-SiO_2 Urubici flows are not a mixture of an Urubici basalt with a low-Ti/Y magma because they have higher Zr contents than the Urubici basalts and the low-Ti/Y basalts or rhyolites (Garland *et al.*, 1995; Peate & Hawkesworth, 1996). Basalt flow 18 has low Zr and lies below the main trend for the Urubici basalts. This, together with its REE and isotopic composition, can be explained if it is a hybrid magma between a unit D Urubici magma and an average Gramado magma.

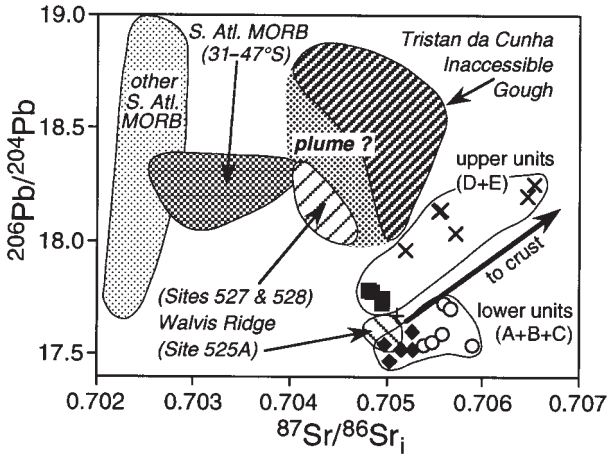

Fig. 10. $^{206}Pb/^{204}Pb$ vs $^{87}Sr/^{86}Sr_i$ diagram for the Urubici basalts, the Tristan plume, Walvis Ridge and South Atlantic MORB. For the Urubici basalts, the lower units (A + B + C) and the upper units (D + E) form two parallel arrays. These are interpreted as reflecting assimilation of high-$^{206}Pb/^{204}Pb$, high-$^{87}Sr/^{86}Sr_i$ crustal material, but in each case starting from compositionally distinct end-members represented by units C and D, respectively. Tristan plume and Walvis Ridge data from Richardson *et al.* (1982), le Roex (1985), Weaver *et al.* (1987), le Roex *et al.* (1990), Cliff *et al.* (1991). South Atlantic MORB data from Hanan *et al.* (1986), Castillo & Batiza (1989), and Fontignie & Schilling (1996). Symbols as in Fig. 5.

upper units also form parallel arrays in Fig. 9a. Hawkesworth *et al.* (1986) noted that the Urubici samples define an apparent isochron on a $^{207}Pb/^{204}Pb$ vs $^{206}Pb/^{204}Pb$ diagram with an age of 1·8 ± 0·4 Ga that is similar to a ^{207}Pb–^{206}Pb age of 2·2 ± 0·2 Ga for the local Precambrian basement rocks. However, any age significance for the source of the Urubici suite as a whole is probably doubtful, given the effects of crustal contamination and mixing shown in Fig. 7. Units C and D have Nd model ages for separation from 'depleted' MORB-source mantle of 1·2–1·3 Ga.

MANTLE ORIGINS OF THE URUBICI MAGMA TYPE

The aims of this section are twofold: (1) to ascertain which compositional features of the Urubici magmas can be attributed to mantle source characteristics; (2) to discuss the composition of melts derived from the Tristan plume and other magmatic samples of the regional upper mantle (lithosphere and asthenosphere), to assess potential sources for the Urubici magmas.

Isotope and trace element characteristics of uncontaminated Urubici magmas

The Urubici magmas have experienced extensive shallow-level processing. They have evolved compositions (*mg*-number <52, Ni <100 ppm) that are far removed from any plausible primary mantle magma {melt in equilibrium with mantle peridotite (*mg*-number 88–89) has *mg*-number 68–75 [*mg*-number is atomic ratio $100 \times Mg/(Mg + Fe^{2+})$ assuming $Fe^{3+}/Fe_{total} = 0{\cdot}15$]; Frey *et al.*, 1978}. To see through the effects of shallow-level crystallization, more reliance is placed on incompatible trace element ratios and isotope compositions. Units C and D are believed to have suffered minimal crustal interaction, by virtue of their low $^{87}Sr/^{86}Sr_i$ and Th/Ta, and from their positions anchoring the low $^{206}Pb/^{204}Pb$ ends of the trends in Figs 5 and 10. Thus, these two units provide the best clues to the nature of the mantle source of the Urubici magma type. The unit B flows are similar in many respects to the unit C flows, but only one sample has been analysed for Sr–Nd–Pb isotopes and by neutron activation analysis and it had higher Th/Ta than the unit C flows.

The trace element characteristics of units C and D are shown in a primitive-mantle-normalized diagram (Fig. 11). Two important features are (1) the depletion in Nb relative to La and K [Nb/La ~0·65 vs 1·0 in normal (N-)MORB], which is not a characteristic of typical oceanic basalts, and (2) the marked depletion of heavy relative to middle rare earth elements (REE) [$(Tb/Yb)_N$ ~2·5], which is indicative of the involvement of residual garnet at some stage during the evolution of the magma or its source: such high $(Tb/Yb)_N$ values are rare in tholeiitic flood basalts. Data for units C and D lie at the low $^{87}Sr/^{86}Sr_i$, high ε_{Nd_i} end of the Urubici array in Fig. 5a. In detail, unit D flows have lower $^{87}Sr/^{86}Sr_i$ and higher ε_{Nd_i} and $^{206}Pb/^{204}Pb$ ($^{87}Sr/^{86}Sr_i$ 0·7048–0·7050, ε_{Nd_i} –1·9 to –2·5, $^{206}Pb/^{204}Pb$ ~17·75) than unit C flows ($^{87}Sr/^{86}Sr_i$ 0·7050–0·7053, ε_{Nd_i} –2·5 to –3·5, $^{206}Pb/^{204}Pb$ ~17·50). Minor trace element differences also exist between these two units (e.g. unit D, Tb/Yb_N ~2·55; unit C, Tb/Yb_N ~2·40) implying a temporal change in the composition of the magma being input to the shallow-level chambers.

Composition of the Tristan mantle plume

The age progressive nature of magmatism along the Walvis Ridge and Rio Grande Rise confirms their interpretation as the fossil magmatic trace of the mantle thermal anomaly, presumably a plume, now located beneath Tristan da Cunha (Fig. 1: O'Connor & Duncan, 1990). The recent (<10 Ma) composition of the plume can be inferred from the magmatism of the Tristan da Cunha island group (Tristan, Inaccessible, Nightingale) and of Gough island, which lies ~500 km to the southeast. Published data (le Roex, 1985; Weaver *et al.*, 1987; le Roex *et al.*, 1990; Cliff *et al.*, 1991) indicate that these islands share many distinctive compositional features that

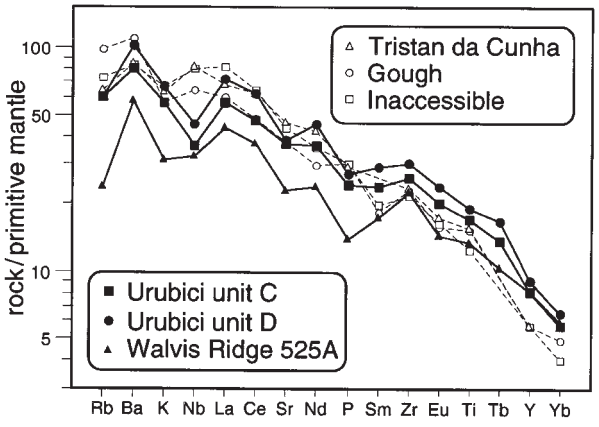

Fig. 11. Primitive-mantle-normalized trace element diagram [normalizing values from Sun & McDonough (1989)]. The patterns for the Urubici basalts and the Walvis Ridge DSDP Site 525A basalts share many similarities, in particular the low Nb/La, which is in marked contrast to the patterns for recent magmas associated with the Tristan plume (Tristan da Cunha, Gough, Inaccessible). Data sources as for Fig. 10, plus Humphris & Thompson (1983) and Sun & McDonough (1989).

distinguish them from most other oceanic islands; e.g. high Ba/La, Ba/Nb and Th/Ta, low ε_{Nd_i} (–4 to +1) and Dupal-type Pb isotope signatures. In detail, there are inter-island differences (Gough and Nightingale have higher $^{207}Pb/^{204}Pb$ for a given $^{206}Pb/^{204}Pb$ value than Tristan and Inaccessible) and some intra-island variations (Inaccessible shows a larger range in ε_{Nd_i} than the other islands) that demonstrate some source heterogeneity (Fig. 12).

Dredging and DSDP drilling have recovered samples from the Walvis Ridge and Rio Grande Rise, but comprehensive isotope and trace element data sets are sparse. Nevertheless, most of the compositional variations can be explained by a mixing model involving a 'depleted' MORB-like mantle source and an 'enriched' mantle source that resembles that of Tristan (Humphris & Thompson, 1983). The DSDP Site 525A basalts (~70 Ma) are an exception and their isotopic values plot away from any possible mixing curves. They have low ε_{Nd_i} (~ –3), low $^{206}Pb/^{204}Pb$ (~17·5), and high Ba/Nb (~17) (Fig. 12: Richardson *et al.*, 1982; Humphris & Thompson, 1983). They also have lower Nb/La than primitive mantle, in contrast to other Walvis Ridge samples and recent Tristan plume magmatism (Figs 11 and 13: Milner & le Roex, 1996). Samples similar to the DSDP Site 525A basalts have been dredged from the eastern part of the Walvis Ridge and drilled at DSDP Site 516F on the Rio Grande Rise (Humphris & Thompson, 1983; Hart, 1984).

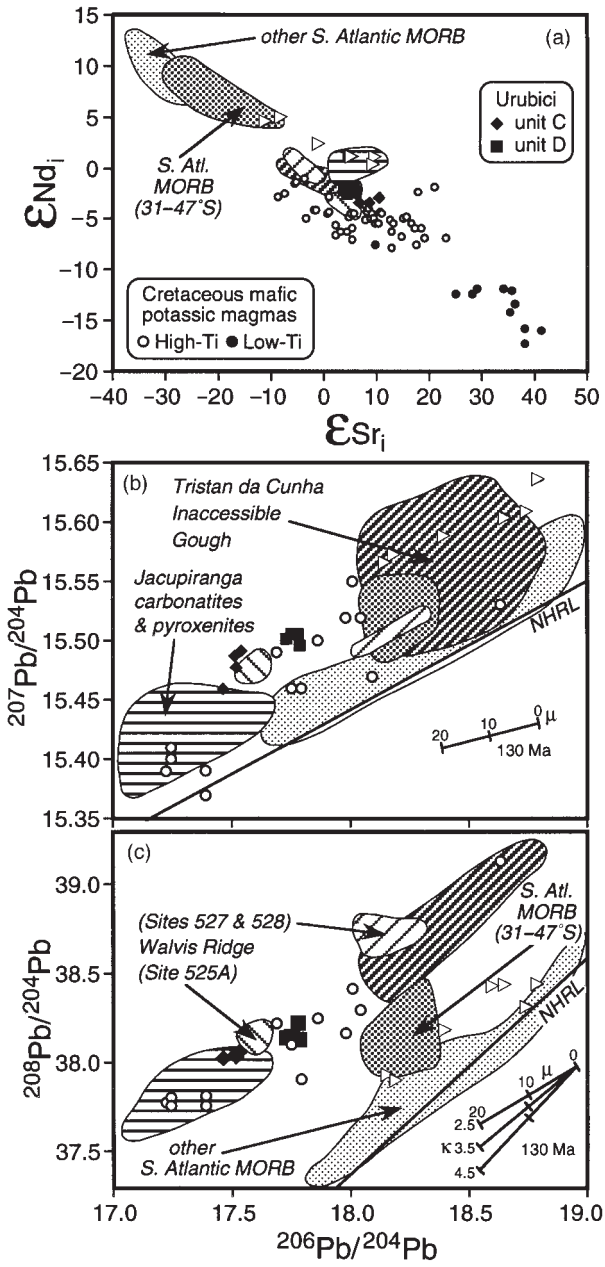

Fig. 12. Radiogenic isotope composition of Cretaceous continental mafic potassic magmas and carbonatites (Toyoda *et al.*, 1994; Gibson *et al.*, 1995*a*, 1995*b*; Huang *et al.*, 1995; Carlson *et al.*, 1996), interpreted as lithospheric mantle melts, and the Tristan plume (Tristan da Cunha, Inaccessible, Gough, Walvis Ridge DSDP Sites 527 and 528: data sources as for Fig. 10), relative to the Urubici unit C and D lavas. (a) ε_{Nd_i} vs ε_{Sr_i}, (b) $^{207}Pb/^{204}Pb$ vs $^{206}Pb/^{204}Pb$, (c) $^{208}Pb/^{204}Pb$ vs $^{206}Pb/^{204}Pb$. Pb isotope data for Cretaceous alkalic magmas are plotted as initial ratios (Alto Paranaíba mafic potassic magmas at 85 Ma, carbonatites at 132 Ma); all other Pb isotope data are measured ratios, but vectors indicate magnitude of age corrections to 130 Ma for different μ ($^{238}U/^{204}Pb$) and κ ($^{232}Th/^{238}U$) values. For most Urubici lavas, μ is ~10 and κ is ~4. Open triangles—Okenyenya alkalic magmas (Milner & le Roex, 1996).

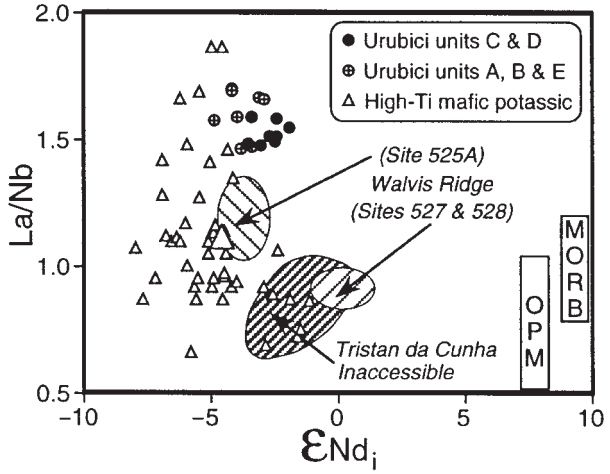

Fig. 13. La/Nb vs ε_{Nd_i} diagram. This illustrates the elevated La/Nb of the Urubici lavas and the Walvis Ridge DSDP Site 525A basalts relative to Tristan plume lavas and other sites on the Walvis Ridge. Furthermore, the Urubici basalts have higher La/Nb than the high-Ti mafic potassic magmas. Data sources as for Fig. 12. OPM is 'oceanic-plume magma' from Gibson *et al.* (1995*a*).

Cretaceous continental alkalic magmatism

The periphery of the Paraná–Etendeka lava field experienced two episodes of compositionally diverse alkalic magmatism during the Cretaceous (124–147 Ma and 55–90 Ma: Ulbrich & Gomes, 1981; Gibson *et al.*, 1995*a*; Milner *et al.*, 1995*b*). Most of this Cretaceous alkalic magmatism is compositionally distinct from recent Tristan plume magmatism, but two exceptions have been described from near the continental margin. The coast-parallel São Sebastião basanitic dykes on the Brazilian coast between São Paulo and Rio de Janeiro (81 Ma: Regelous, 1993; SJII dykes of Hawkesworth *et al.*, 1992) have Tristan-like incompatible trace element patterns and Sr–Nd–Pb isotope compositions. The presence of the São Sebastião dykes, together with the bulk of the Walvis Ridge data, is strong evidence that the composition of at least one type of mantle in the Tristan plume has not changed significantly over at least the last 90 my. Milner & le Roex (1996) considered the alkalic magmas from Okenyenya, Namibia (Fig. 1: 124–130 Ma) to be compositionally similar to modern Tristan plume magmas, but these magmas have significantly lower $^{208}Pb/^{204}Pb$ than the main Tristan plume field (Fig. 12).

Several of the Early Cretaceous carbonatite complexes [Jacupiranga, ~250 km north of São Joaquim (Fig. 2), and Anitapolis, 90 km east of São Joaquim (Fig. 4)] have low $^{206}Pb/^{204}Pb$ compositions similar to the Urubici and Walvis Ridge DSDP Site 525A basalts. The distinctive isotope characteristics of Jacupiranga (Dupal Pb isotopes and Sr and Nd isotope compositions close to estimated Bulk Earth values: $^{87}Sr/^{86}Sr_i$ 0·7047–0·7057, ε_{Nd_i} +1·6 to −1·2, $^{206}Pb/^{204}Pb$ 17·0–17·7: Toyoda *et al.*, 1994; Huang *et al.*, 1995) are inferred to be a mantle source feature, given the high trace element contents of the samples and the mantle-like $\delta^{18}O$ values. Carbonatitic dykes at Anitapolis have slightly higher $\delta^{18}O$, $^{87}Sr/^{86}Sr_i$ and $^{206}Pb/^{204}Pb_i$ values than Jacupiranga, indicating a limited interaction with upper-crustal material (Toyoda *et al.*, 1994).

Gibson *et al.* (1995*a*) recognized that the Cretaceous mafic potassic magmatism can be divided into two compositionally and geographically distinct groups: (1) a high-Ti group (TiO_2 ~4·6 wt %) with high ε_{Nd_i} (~ −5) and low La/Nb (~1·1) and $^{87}Sr/^{86}Sr_i$ (~0·7050), found along the northeast margin of the Paraná lava field, associated with the Proterozoic mobile belts, and (2) a low-Ti group (TiO_2 ~1·8 wt %) with low ε_{Nd_i} (~ −13) and high La/Nb (~2·0) and $^{87}Sr/^{86}Sr_i$ (~0·7068), found adjacent to the central Paraná lavas along the coast in the east and in Paraguay to the west, associated with cratonic regions. Mafic potassic magmas are widely accepted as representing small degree melts of the lithospheric mantle. Gibson *et al.* (1995*a*) concluded that the spatial distribution of high-Ti and low-Ti mafic potassic rocks was analogous to the high-Ti–low-Ti provinciality seen in the Paraná basalts and reflected a major compositional change in the continental lithospheric mantle, as previously suggested on the basis of the basalt data by Erlank *et al.* (1988) and Hawkesworth *et al.* (1988). However, this boundary might not be the same as that inferred from the basalts. The low-Ti mafic potassic rocks are spatially associated with tholeiitic dykes that are inferred to be the feeder systems to the volumetrically dominant northern high-Ti/Y flood basalts (Fig. 2), and yet the strike of the tholeiitic dykes is roughly parallel to the inferred lithospheric mantle boundary of Gibson *et al.* (1995*a*).

Carlson *et al.* (1996) showed that the high-Ti mafic potassic magmas in the Alto Paranaíba region (Fig. 1) generally have low $^{206}Pb/^{204}Pb_{85Ma}$ (17·2–18·1) and elevated $^{208}Pb/^{204}Pb_{85Ma}$ (37·8–38·6) (Fig. 12). Some of the lamproitic and kimberlitic samples have extremely low $^{187}Os/^{188}Os_i$ (0·112–0·121), lower than oceanic basalts and abyssal peridotites, and such characteristics are apparently unique to peridotitic lithospheric mantle sources that experienced melt-related Re depletion during the Archaean or Proterozoic (Carlson *et al.*, 1996). Kamafugitic samples have high $^{187}Os/^{188}Os_i$ (0·27–0·31), but the high Os contents rule out the possibility of contamination with old, high-Re/Os crustal material, and instead Carlson *et al.* (1996) interpreted them as being derived from a pyroxenitic or eclogitic source within the lithospheric mantle. Thus, Carlson *et al.* (1996) argued that the Sr–Nd–Pb–Os isotopic characteristics of the Alto Paranaíba samples were inherited from diverse sources within the lithospheric mantle and were not compatible with a mantle source that had been modified by melts from the Tristan plume.

A common mantle source for high-Ti/Y and low-Ti/Y magma types?

To understand the mantle origins of the high-Ti/Y Urubici magma type, we should also consider its relationship to the contemporaneous low-Ti/Y magmatism. These two types cannot be related by crustal-level processes such as crystallization or assimilation. Fodor (1987) and Arndt *et al.* (1993) considered that coexisting high- and low-Ti/Y basalts in the Paraná and in other flood basalt provinces could be linked simply by different degrees of melting of a common mantle source, the higher incompatible trace element contents of the high-Ti/Y magmas reflecting lower degrees of melting than for the low-Ti/Y magmas. Fodor (1987) related the melting differences to the proximity of the underlying Tristan plume, with low-Ti/Y basalts over the hot plume axis in the south and high-Ti/Y basalts on the cooler plume periphery to the north. Following McKenzie & Bickle (1988), Arndt *et al.* (1993) considered lithospheric thickness to be the principal factor in determining the degree and depth of melting, by controlling the extent to which the underlying asthenospheric mantle can decompress and melt; it should be noted that melting of the lithospheric mantle is not the main issue here. Beneath thick lithosphere, the degree of melting will be limited and will occur at high pressure in the presence of residual garnet, thus leading to incompatible-element-enriched basalts with high Ti/Y and Tb/Yb. If similar source material ascends to shallower depths beneath a lithosphere perhaps thinned by extension, the degree of melting will be higher, producing melts with lower concentrations of incompatible elements and without a residual garnet signature (i.e. low Ti/Y and Tb/Yb). The difference in Tb/Yb between the low-Ti/Y and high-Ti/Y magmas is illustrated in Fig. 14b. In some flood basalt provinces, there is a temporal switch from high-Ti/Y and -Tb/Yb lavas to low-Ti/Y and -Tb/Yb lavas (e.g. Ellam, 1992; Fram & Lesher, 1993; White & McKenzie, 1995), consistent with progressive lithospheric thinning during rifting. In the Paraná–Etendeka province, it is important to note that the high-Ti/Y Urubici and low-Ti/Y Gramado magma types are contemporaneous, which would require significant lateral variations in lithospheric thickness along the developing South Atlantic rift in such a model, and yet both types appear to have been erupted from coast-parallel dykes. Any isotopic differences between the high-Ti/Y and low-Ti/Y types, or relative to typical asthenospheric melts, were simply attributed to crustal contamination by Fodor (1987) and Arndt *et al.* (1993). It remains difficult, though, to reconcile the isotopic variations of the Paraná lavas in terms of melts from a single mantle source without appealing to models that require melts derived from contrasting pressure and/or temperature conditions to also assimilate compositionally different crustal components.

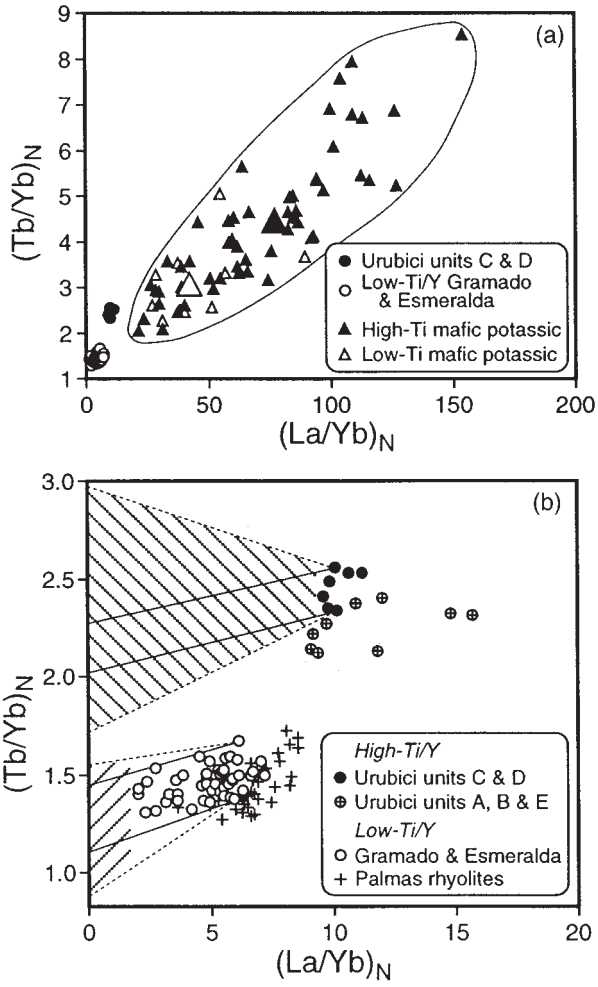

Fig. 14. (a) $(Tb/Yb)_N$ vs $(La/Yb)_N$ diagram illustrating the REE characteristics of the high-Ti and low-Ti mafic potassic magmas (Gibson *et al.*, 1995*a*, 1995*b*; Carlson *et al.*, 1996) relative to the high-Ti/Y and low-Ti/Y flood basalts (Table 2; Peate & Hawkesworth, 1996). The large symbols represent average compositions for the high-Ti (filled) and low-Ti (open) mafic potassic magmas. (b) An enlargement of bottom left-hand corner of (a). If the compositions of the high-Ti/Y and low-Ti/Y Paraná basalts represent mixtures of an asthenospheric melt with high-Ti and low-Ti mafic potassic magmas, respectively (Gibson *et al.*, 1995*a*), then the composition of the asthenospheric melt must lie within the shaded regions. It is clear that, for this model, the asthenosphere-derived end-member must be different for the high-Ti/Y and low-Ti/Y basalts. The continuous lines show the low $(La/Yb)_N$ portions of mixing trends to the average high-Ti and low-Ti mafic potassic magmas, and the dashed lines represent mixing with the extremes of observed mafic potassic magma compositions.

In certain flood basalt provinces, close compositional similarities exist between some of the flood basalt flows and the recent oceanic magmatism of the associated mantle plume (e.g. Deccan flood basalts and Réunion plume, Mahoney, 1988: Madagascar flood basalts and Marion plume, Mahoney *et al.*, 1991; Storey *et al.*, 1997:

Greenland flood basalts and Iceland plume, Thirlwall *et al.*, 1994). However, it has proven more difficult to demonstrate a similar compositional link between the Paraná–Etendeka flood basalts and the youngest magmatic products of the Tristan mantle plume (Hawkesworth *et al.*, 1992; Peate & Hawkesworth, 1996). The high-Ti/Y Urubici lavas have Nb troughs on primitive-mantle-normalized trace element plots, which are not a feature of the modern Tristan plume (Fig. 11), and the isotopic differences between these flood basalts and both recent plume-derived magmas and local MORB-source asthenosphere are apparent from comparing the data in Figs 5 and 12. Instead, the Urubici basalts have more compositional features in common with those Cretaceous alkalic magmas that are inferred to be small-degree melts of the continental lithospheric mantle.

A ROLE FOR LITHOSPHERIC MANTLE?

It has been proposed that the lithospheric mantle plays an important role in magma genesis in some, but not all, flood basalt provinces (e.g. Allègre *et al.*, 1982; Hawkesworth *et al.*, 1984, 1988; Ellam & Cox, 1991; Hergt *et al.*, 1991; Ellam *et al.*, 1992; Sweeney *et al.*, 1994; Gibson *et al.*, 1995*a*; Molzahn *et al.*, 1996; Peate & Hawkesworth, 1996; Turner *et al.*, 1996; Lassiter & DePaolo, 1997). These ideas were influenced primarily by studies of the Mesozoic Gondwanan flood basalt provinces (Paraná–Etendeka, Karoo, Ferrar) and emphasized two important features of these basalts: (1) samples considered to be uncontaminated by crust had trace element and isotope characteristics distinct from typical oceanic basalts, namely, low Nb/La and ε_{Nd_i} and high $^{87}Sr/^{86}Sr_i$, with a virtual absence (<5%) of any samples with ε_{Nd_i} values higher than Bulk Earth (e.g. Hawkesworth *et al.*, 1984, 1988; Hergt *et al.*, 1991; Peate *et al.*, 1992; Sweeney *et al.*, 1994); (2) high-Ti/Y and low-Ti/Y flood basalts form spatially distinct geochemical provinces that can be traced throughout the former Gondwana supercontinent (Bellieni *et al.*, 1984; Erlank *et al.*, 1988; Hergt *et al.*, 1991). ^{40}Ar–^{39}Ar ages suggest that the stratigraphic units defined by the Paraná basalt magma types are not chronostratigraphic (Turner *et al.*, 1994), and Peate *et al.* (1990) showed that they were erupted from different centres. Thus the spectrum of magma compositions cannot represent the temporal evolution of a single mantle source region. The surface distribution of magma types appears to reflect the subcrustal distribution of distinct lithospheric source regions (Hawkesworth *et al.*, 1988), similar to the lithospheric mantle provinciality inferred from the Cretaceous alkalic magmatism (Gibson *et al.*, 1995*a*).

Assimilation of small-degree lithospheric melts by plume-derived melts?

One mechanism by which the lithospheric mantle could contribute to flood basalt magmatism is by asthenospheric melts assimilating a lithospheric mantle component, either as they migrate up through the lithosphere or via thermal erosion of the base of the lithosphere by an incubating plume head (e.g. McKenzie, 1989; Ellam & Cox, 1991; Saunders *et al.*, 1992). This component is inferred to be in the form of low-melting-point hydrous and carbonated material similar in composition to mafic potassic magmas. Ellam *et al.* (1992) presented good evidence for such a model to explain the positive correlations between Nd, Pb, and Os isotope compositions in the high-Ti Nuanetsi picrites (Karoo flood basalt province, southern Africa). The low ε_{Nd_i} (~ –10), low $^{206}Pb/^{204}Pb_i$ (~17·4) end-member has low $^{187}Os/^{188}Os_i$ (<0·123), indicative of an incompatible-trace-element-enriched lithospheric mantle component rather than crust.

Gibson *et al.* (1995*a*) tried to model the composition of the Paraná high-Ti and low-Ti basalts by mixing between an asthenospheric melt and the Cretaceous high-Ti and low-Ti mafic potassic lithospheric melts, respectively, followed in both cases by extensive crystallization and crustal assimilation. The asthenospheric end-member was assumed to be similar to the incompatible-trace-element-depleted tholeiitic and picritic lavas found on Iceland and on the Caribbean oceanic plateau, which are interpreted as large degree melts, formed by shallow decompression and/or elevated mantle temperatures, of a depleted mantle component within the plume head, referred to by Gibson *et al.* (1995*a*) as 'oceanic plume magmas'. It is not clear, though, that lithospheric extension was sufficient to allow decompression to such shallow depths during this stage of the Paraná–Etendeka magmatism (e.g. Turner *et al.*, 1996). Gibson *et al.* (1995*a*) suggested that the Sr and Nd isotopic composition of the high-Ti/Y flood basalts was consistent with the addition of ~50% high-Ti mafic potassic lithospheric-derived melt to an 'oceanic plume magma'.

One problem with this model is highlighted by the REE data (Fig. 14). Both of the axes in this plot [$(Tb/Yb)_N$ vs $(La/Yb)_N$] have the same denominator and so binary mixing is linear. It is possible to extrapolate mixing lines from the high-Ti mafic potassic magmas through the field of the Urubici magmas to define the region where an asthenospheric end-member must lie in the model of Gibson *et al.* (1995*a*). A similar procedure can be done for the low-Ti mafic potassic magmas and the low-Ti/Y flood basalts. It is clear that the difference in $(Tb/Yb)_N$ between the contemporaneous high-Ti/Y and low-Ti/Y basalts cannot be explained by addition of

mafic potassic melts of different REE composition to a common asthenospheric melt end-member: this problem is not mitigated by the effects of crustal contamination on the Urubici magmas because the contaminated units (A, B, E) have lower $(Tb/Yb)_N$. The model of Gibson *et al.* (1995*a*) thus requires significant contemporaneous differences in the asthenospheric melting conditions to produce compositionally different parental melts to the Urubici magmas [asthenospheric melt with $(Tb/Yb)_N$ ~2·0] and the Gramado magmas [asthenospheric melt with $(Tb/Yb)_N$ ~1·3].

The least contaminated Urubici units C and D flows have a broadly similar Nd isotope composition (ε_{Nd_i} –2·7 ± 0·6) to the high-Ti mafic potassic melts (ε_{Nd_i} –4·8 ± 1·6: Gibson *et al.*, 1995*a*, 1995*b*; Carlson *et al.*, 1996), but they have much higher La/Nb (1·6 vs 1·1), a difference attributed by Gibson *et al.* (1995*a*) to crustal assimilation. Given that the local Brazilian crust has $\varepsilon_{Nd_{130Ma}} < -10$, the significant crustal addition that would be required to explain the difference in La/Nb would mean that the uncontaminated Urubici magmas would have $\varepsilon_{Nd_i} > 0$, which then limits the amount of lamproitic addition possible. The available $\delta^{18}O$ data argue against significant crustal contamination, and the Pb isotope data for the Urubici magmas are similar to values for the Cretaceous mafic potassic lithospheric melts.

The marked compositional similarities, both in terms of trace elements and radiogenic isotopes, between the Walvis Ridge DSDP Site 525A basalts and the Urubici magma type of the Paraná flood basalts mean that it is difficult to escape the conclusion that ultimately both are derived from a common mantle source. Whichever petrogenetic model is chosen for the origins of the compositional features of the Urubici magma type has important implications for the nature and original location of the enriched mantle component (EM1) seen in the Walvis Ridge DSDP Site 525A basalts, and vice versa, a point also made by Hawkesworth *et al.* (1986), Toyoda *et al.* (1994) and Milner & le Roex (1996). Any model that invokes crustal contamination to account for the compositional features of the Urubici magmas must then address the compositional coincidence between the Urubici samples and the DSDP Site 525A Walvis Ridge samples. Another possibility is that the Urubici basalts represent wholesale melting of hydrated Brazilian lithospheric mantle, and the DSDP Site 525A Walvis Ridge lavas sample similar material that was delaminated during break-up and entrained in the asthenosphere.

Melting of hydrated lithospheric mantle peridotite

If melting occurs at the anhydrous peridotite solidus during continental rifting above a mantle plume then >95% of melt produced will be of asthenospheric origin, as proposed by, for example, McKenzie & Bickle (1988) and Arndt & Christensen (1992). However, those workers did not consider the implications of a plume incubating beneath thick lithosphere for several million years or the presence of small amounts of water within the lithospheric mantle. Gallagher & Hawkesworth (1992) and Turner *et al.* (1996) demonstrated that melting will then preferentially occur at the volatile-enriched solidus within the lithospheric mantle unless there is significant extension to facilitate adiabatic decompression melting of the underlying asthenosphere. A key issue is the thickness of the lithosphere at the time of magmatism. If the lithospheric thickness is >130 km and extension remains low, as appears to be the case in the Paraná (Turner *et al.*, 1996), then melting will be confined to the lithospheric mantle [see also Storey *et al.* (1997)].

IMPLICATIONS FOR THE LOCATION OF 'DUPAL-ANOMALY' MANTLE AND 'EM1-TYPE' MANTLE IN THE SOUTH ATLANTIC REGION

Hart (1984) defined the Dupal mantle anomaly in the South Atlantic region on the basis of the distinctive isotopic compositions of lavas from some geographically adjacent oceanic islands, aseismic ridges, and seamount chains, which include Tristan, Gough, Walvis Ridge and Rio Grande Rise. These OIB also share several trace element features, such as high Ba/Nb and Ba/La, that are distinct from most other OIB and MORB (e.g. Weaver *et al.*, 1987). The implication is that these OIB all sample a similar, isotopically anomalous, mantle source. This is surprising, given the wide range in, for example, $^{206}Pb/^{204}Pb$ (17·5–18·8), which cannot easily be explained by variable entrainment of MORB-source asthenospheric material in any plume upwelling (e.g. Fig. 12c). This point is best illustrated by the isotopic data from the Walvis Ridge (Richardson *et al.*, 1982), which, in many publications, are portrayed as a linear array. In fact, as stressed by Milner & le Roex (1996), the Walvis Ridge data form two distinct groups, one broadly similar to data for recent Tristan plume lavas and the other with low $^{206}Pb/^{204}Pb$, EM1-type features, but with both groups showing Dupal isotope characteristics. Low $^{206}Pb/^{204}Pb$ material apparently has a rather restricted distribution offshore, being found only at DSDP Site 525A on the Walvis Ridge (Richardson *et al.*, 1982) and Site 519 on the Rio Grande Rise (Hart, 1984), although more detailed isotopic coverage of the Walvis Ridge and the Rio Grande Rise is clearly required. This material is not involved in the mixing arrays defined by most other Walvis Ridge samples, which reflect interaction between Tristan-like

plume material and MORB source asthenosphere (Richardson *et al.*, 1982; Humphris & Thompson, 1983). Similarly, MORB from the nearby Mid-Atlantic Ridge (22°–31°S) do not contain any trace of this low $^{206}Pb/^{204}Pb$ material (e.g. Figs 9 and 12c), although their compositions are consistent with the plume–ridge interaction model outlined by Humphris *et al.* (1985), Hanan *et al.* (1986) and Fontignie & Schilling (1996), using data from Tristan and Gough to represent the plume end-member. Where low $^{206}Pb/^{204}Pb$ material is found in South Atlantic MORB, further south at 48·5°–49·0°S and 52·3°–52·7°S, it appears to be isolated and not mixed with plume or asthenospheric material (Douglass *et al.*, 1996). An analogous situation is found along the Southwest Indian Ridge at 39°–41°S, where low $^{206}Pb/^{204}Pb$ compositions are also difficult to ascribe to plume–ridge interactions, in this case involving the Marion plume (Mahoney *et al.*, 1992). Thus, in the South Atlantic region, it is not obvious that the low $^{206}Pb/^{204}Pb$, EM1-type mantle is part of the Tristan plume upwelling, unless one resorts to the rather *ad hoc* explanation that it was present early in the history of the Tristan plume but is now exhausted or just a very minor component.

Since the paper of Hawkesworth *et al.* (1986) that discussed the possible link between the Paraná high-Ti/Y flood basalts and the Dupal oceanic magmatism in terms of delaminated lithospheric mantle, data have been published from unambiguous samples of the Brazilian continental mantle lithosphere in the form of Cretaceous small-degree mafic potassic melts (Gibson *et al.*, 1995*a*; Carlson *et al.*, 1996). From these, it is clear that the distinctive compositional features of the uncontaminated Urubici magmas are also seen in many samples derived from the local Brazilian mantle lithosphere, and this strengthens the case for a lithospheric mantle origin both for these high-Ti/Y flood basalts and, indirectly, the DSDP Site 525A Walvis Ridge samples. The data for the Cretaceous alkalic rocks show that the regional continental lithospheric mantle is isotopically fairly heterogeneous (Fig. 12), and thus is not itself equivalent to the EM1 component as originally defined by Zindler & Hart (1986): its range of $^{206}Pb/^{204}Pb$ goes well below the values seen in the Site 525A lavas. In detail, more than one low $^{206}Pb/^{204}Pb$ 'component' is required, given the significant range in $^{207}Pb/^{204}Pb$ even at the lowest $^{206}Pb/^{204}Pb$, and Mahoney *et al.* (1996) reached a similar conclusion for Indian Ocean MORB and OIB.

It is likely that material from the base of the continental mantle lithosphere is detached during continental breakup, perhaps enhanced by plume-driven thermal erosion, and is subsequently dispersed within the shallow asthenosphere by secondary convection processes during seafloor spreading (e.g. Hawkesworth *et al.*, 1986; Douglass *et al.*, 1996; Milner & le Roex, 1996). The South Atlantic region is not an isolated example, and a similar model has been proposed to account for the compositional and spatial variations documented within the Madagascar flood basalts–Marion plume–Southwest Ridge Indian MORB system (Mahoney *et al.*, 1991, 1992; Storey *et al.*, 1997). The similarities between this system and the South Atlantic region have been discussed in detail by Milner & le Roex (1996).

The Tristan plume is probably a relatively deep mantle upwelling, and Castillo (1988) linked it to a low seismic velocity anomaly in the lower mantle. The 'enriched' incompatible trace element and isotopic characteristics of the Tristan plume might ultimately also be derived from continental lithospheric mantle material (e.g. le Roex, 1986; Hofmann, 1997), which, in contrast to the DSDP Site 525A source, has been cycled relatively deep in the mantle convection system and brought up as an intrinsic part of the plume. In conclusion, we prefer a model in which the Dupal anomaly in the South Atlantic region, in fact, is two distinct entities [see also Milner & le Roex (1996)]; one shallow in origin (low $^{206}Pb/^{204}Pb$, high Ba/Nb delaminated rafts of local lithospheric mantle as sampled at DSDP Site 525A) and the other deep in origin (Tristan plume).

ACKNOWLEDGEMENTS

This study began as part of an NERC-supported Ph.D. project by D.W.P. at the Open University. Andy Duncan kindly provided unpublished analyses of the Khumib basalts in the Etendeka for comparison. Peter van Calsteren, Mabs Gilmour, Tim Brewer and John Watson are thanked for their assistance with the analytical work. Discussions with Janet Hergt, Mukul Sharma and Michael Storey on flood basalts were enlightening. Keith Cox and Steve Blake provided some pertinent comments on an earlier version of the manuscript when it existed as a thesis chapter. We thank John Mahoney, Rick Carlson and Rob Ellam, for their reviews. The detailed comments of John Mahoney were especially helpful in improving the final manuscript. Isotope research at the Open University is partly supported by NERC. We acknowledge the financial support of FAPESP and CNPq to Marta Mantovani for logistical support during fieldwork, and also the support during manuscript preparation from the Danish Lithosphere Centre, which is funded by the Danish National Research Foundation.

REFERENCES

Allègre, C. J., Dupre, B., Richard, P., Rousseau, D. & Brooks, C. (1982). Subcontinental versus suboceanic mantle, II. Nd–Sr–Pb isotopic comparison of continental tholeiites with mid-ocean ridge tholeiites, and the structure of the continental lithosphere. *Earth and Planetary Science Letters* **57,** 25–34.

Arndt, N. T. & Christensen, U. (1992). The role of lithospheric mantle in the generation of continental flood basalts. *Journal of Geophysical Research* **97,** 10967–10981.

Arndt, N. T., Czamanske, G. K., Wooden, J. L. & Federenko, V. A. (1993). Mantle and crustal contributions to continental flood volcanism. *Tectonophysics* **223,** 39–52.

Bellieni, G., Comin-Chiaramonti, P., Marques, L. S., Melfi, A. J., Piccirillo, E. M., Nardy, A. J. R. & Roisenberg, A. (1984). High- and low-Ti flood basalts from the Paraná plateau (Brazil): petrology and geochemical aspects bearing on their mantle origin. *Neues Jahrbuch für Mineralogie, Abhandlungen* **150,** 272–306.

Carlson, R. W., Esperança, S. & Svisero, D. (1996). Chemical and Os isotopic study of Cretaceous potassic rocks from Southern Brazil. *Contributions to Mineralogy and Petrology* **125,** 393–405.

Castillo, P. (1988). The Dupal anomaly as a trace of the upwelling lower mantle. *Nature* **336,** 667–670.

Castillo, P. & Batiza, R. (1989). Strontium, neodymium and lead isotope constraints on near-ridge seamount production beneath the South Atlantic. *Nature* **342,** 262–265.

Cliff, R. A., Baker, P. E. & Mateer, N. J. (1991). Geochemistry of Inaccessible Island volcanics. *Chemical Geology* **92,** 251–260.

Comin-Chiaramonti, P., Bellieni, G., Piccirillo, E. M. & Melfi, A. J. (1988). Classification and petrography of continental stratoid volcanics and related intrusives from the Paraná basin (Brazil). In: Piccirillo, E. M. & Melfi, A. J. (eds) *The Mesozoic Flood Volcanism of the Paraná Basin: Petrogenetic and Geophysical Aspects*. São Paulo: IAG-USP Press, pp. 47–72.

Cox, K. G. (1980). A model for flood basalt volcanism. *Journal of Petrology* **21,** 629–650.

de Oliveira, A. V. (1956). Brazil. In: Jenks, W. F. (ed.) *Handbook of South American Geology. Geological Society of America, Memoir* **65,** 1–62.

DePaolo, D. J. (1981). Trace element and isotopic effects of combined wall rock assimilation and fractional crystallisation. *Earth and Planetary Letters* **53,** 189–202.

Douglass, J., Schilling, J.-G. & Fontignie, D. (1996). The Discovery and Shona mantle plumes and the Lo-Mu component: an inexorable connection? *Eos Transactions, American Geophysical Union* **77,** F827.

Duncan, A. R. (1987). The Karoo igneous province—a problem area for inferring tectonic setting from basalt geochemistry. *Journal of Volcanology and Geothermal Research* **32,** 13–34.

Ellam, R. E. (1992). Lithospheric thickness as a control on basalt geochemistry. *Geology* **20,** 153–156.

Ellam, R. M. & Cox, K. G. (1991). An interpretation of Karoo picrite basalts in terms of interaction between asthenospheric magmas and mantle lithosphere. *Earth and Planetary Science Letters* **105,** 330–342.

Ellam, R. M., Carlson, R. W. & Shirey, S. B. (1992). Evidence from Re–Os isotopes for plume–lithosphere mixing in Karoo flood basalt genesis. *Nature* **359,** 718–721.

Erlank, A. J., Duncan, A. R., Marsh, J. S., Sweeney, R. S., Hawkesworth, C. J., Milner, S. C., Miller, R. & Rogers, N. W. (1988). A laterally extensive geochemical discontinuity in the sub-continental Gondwana lithosphere. *Conference on Geochemical Evolution of the Continental Crust, Poços de Caldas, Brazil. Abstracts Volume*. São Paulo: University of São Paulo, pp. 1–9.

Fodor, R. V. (1987). Low- and high-TiO_2 flood basalts of southern Brazil: origin from a picritic parentage and a common mantle source. *Earth and Planetary Science Letters* **84,** 423–430.

Fontignie, D. & Schilling, J.-G. (1996). Mantle heterogeneities beneath the South Atlantic: a Nd–Sr–Pb isotope study along the Mid-Atlantic Ridge (3°S–46°S). *Earth and Planetary Science Letters* **142,** 209–221.

Fram, M. S. & Lesher, C. E. (1993). Geochemical constraints on mantle melting during creation of the North Atlantic basin. *Nature* **363,** 712–715.

Frey, F. A., Green, D. H. & Roy, S. D. (1978). Integrated models of basalt petrogenesis: a study of quartz tholeiites to olivine melilities from south eastern Australia utilising geochemical and experimental petrological data. *Journal of Petrology* **19,** 463–513.

Gallagher, K. & Hawkesworth, C. J. (1992). Dehydration melting and the generation of continental flood basalts. *Nature* **358,** 57–59.

Gallagher, K., Hawkesworth, C. J. & Mantovani, M. S. M. (1994). The denudation history of the onshore continental margin of SE Brazil inferred from apatite fission track data. *Journal of Geophysical Research* **99,** 18117–18145.

Garland, F., Hawkesworth, C. J. & Mantovani, M. S. M. (1995). Description and petrogenesis of the Paraná rhyolites, southern Brazil. *Journal of Petrology* **36,** 1193–1227.

Ghiorso, M. S. & Sack, R. O. (1995). Chemical mass transfer in magmatic process. IV. A revised and internally consistent thermodynamic model for the interpretation and extrapolation of liquid–solid equilibria in magmatic systems at elevated temperatures and pressures. *Contributions to Mineralogy and Petrology* **119,** 197–212.

Gibson, S. A., Thompson, R. N., Dickin, A. P. & Leonardos, O. H. (1995*a*). Mafic potassic magmatic key to plume–lithosphere interactions and continental flood-basalts. *Earth and Planetary Science Letters* **136,** 149–165.

Gibson, S. A., Thompson, R. N., Leonardos, O. H., Dickin, A. P. & Mitchell, J. G. (1995*b*). The Late Cretaceous impact of the Trinidade mantle plume: evidence from large volume, mafic potassic magmatism in SE Brazil. *Journal of Petrology* **36,** 189–229.

Hanan, B. B., Kingsley, R. H. & Schilling, J.-G. (1986). Pb isotope evidence in the South Atlantic for migrating ridge–hotspot interactions. *Nature* **332,** 137–144.

Harris, C., Smith, H. C., Milner, S. C., Erlank, A. J., Duncan, A. R., Marsh, J. S. & Ikin, N. P. (1989). Oxygen isotope geochemistry of the Mesozoic volcanics of the Etendeka Formation, Namibia. *Contributions to Mineralogy and Petrology* **102,** 454–461.

Hart, S. R. (1984). A large-scale isotope anomaly in the southern hemisphere mantle. *Nature* **309,** 753–757.

Hawkesworth, C. J., Marsh, J. S., Duncan, A. R., Erlank, A. J. & Norry, M. J. (1984). The role of continental lithosphere in the generation of the Karoo volcanic rocks: evidence from combined Nd- and Sr-isotope studies. In: Erlank, A. J. (ed.) *Petrogenesis of the Volcanic Rocks of the Karoo Province. Special Publication of the Geological Society of South Africa* **13,** 341–354.

Hawkesworth, C. J., Mantovani, M. S. M., Taylor, P. N. & Palacz, Z. (1986). Evidence from the Paraná of south Brazil for a continental contribution to Dupal basalts. *Nature* **322,** 356–359.

Hawkesworth, C. J., Mantovani, M. S. M. & Peate, D. W. (1988). Lithosphere remobilization during Paraná magmatism. *Journal of Petrology (Special Lithosphere Issue)* 205–233.

Hawkesworth, C. J., Gallagher, K., Kelley, S., Mantovani, M. S. M., Peate, D. W., Regelous, M. & Rogers, N. W. (1992). Paraná magmatism and the opening of the South Atlantic. In: Storey, B. C., Alabaster, A. & Pankhurst, R. J. (eds) *Magmatism and the Cause of Continental Break-up. Geological Society, London, Special Publication* **68,** 221–240.

Hergt, J. M., Peate, D. W. & Hawkesworth, C. J. (1991). The petrogenesis of Mesozoic Gondwana low-Ti flood basalts. *Earth and Planetary Letters* **105,** 134–148.

Hofmann, A. W. (1997). Mantle geochemistry: the message from oceanic volcanism. *Nature* **385,** 219–229.

Huang, Y.-M., Hawkesworth, C. J., van Calsteren, P. W. & McDermott, F. (1995). Geochemical characteristics and origin of the Jacupiranga carbonatites, Brazil. *Chemical Geology* **119,** 79–99.

Humphris, S. E. & Thompson, G. (1983). Geochemistry of rare earth elements in basalts from the Walvis Ridge: implications for its origin and evolution. *Earth and Planetary Science Letters* **66,** 223–242.

Humphris, S. E., Thompson, G., Schilling, J.-G. & Kingsley, R. H. (1985). Petrological and geochemical variations along the Mid-Atlantic Ridge between 46°S and 32°S: influence of the Tristan da Cunha mantle plume. *Geochimica et Cosmochimica Acta* **49,** 1445–1464.

Iacumin, P., Piccirillo, E. M. & Longinelli, A. (1991). Oxygen isotopic composition of Lower Cretaceous tholeiites and Precambrian basement rocks from the Paraná basin (Brazil): the role of water–rock interaction. *Chemical Geology (Isotope Geoscience Section)* **86,** 225–237.

Lassiter, J. C. & DePaolo, D. J. (1997). Plume/lithosphere interaction in the generation of continental and oceanic flood basalts: chemical and isotopic constraints. In: Mahoney, J. J. & Coffin, M. F. (eds) *Large Igneous Provinces: Continental, Oceanic, and Planetary Flood Volcanism. Geophysical Monograph, American Geophysical Union* **100,** 335–355.

le Roex, A. P. (1985). Geochemistry, mineralogy, and magmatic evolution of the basaltic and trachytic lavas from Gough Island, South Atlantic. *Journal of Petrology* **26,** 149–186.

le Roex, A. P. (1986). Geochemical correlation between southern African kimberlites and South Atlantic hotspots. *Nature* **324,** 243–245.

le Roex, A. P., Cliff, R. A. & Adair, B. (1990). Tristan da Cunha, South Atlantic: geochemistry and petrogenesis of a basanite–phonolite lava series. *Journal of Petrology* **31,** 779–812.

Mahoney, J. J. (1988). Deccan Traps. In: Macdougall, J. D. (ed.) *Continental Flood Basalts*. Dordrecht: Kluwer, pp. 151–194.

Mahoney, J. J., Nicollet, C. & Dupuy, C. (1991). Madagascar basalts: tracking oceanic and continental sources. *Earth and Planetary Science Letters* **104,** 350–363.

Mahoney, J. J., le Roex, A. P., Peng, Z., Fisher, R. L. & Natland, J. H. (1992). Southwestern limits of Indian Ocean Ridge mantle and the origin of low $^{206}Pb/^{204}Pb$ mid-ocean ridge basalt: isotope systematics of the central Southwest Indian Ridge (17°–50°E). *Journal of Geophysical Research* **97,** 19771–19790.

Mahoney, J. J., White, W. M., Upton, B. G. J., Neal, C. R. & Scrutton, R. A. (1996). Beyond EM-1: lavas from Afanasy–Nikitin Rise and the Crozet archipelago, Indian Ocean. *Geology* **24,** 615–618.

Mantovani, M. S. M., Marques, L. S., De Sousa, M. A., Civetta, L., Atalla, L. & Innocenti, F. (1985). Trace element and strontium isotope constraints on the origin and evolution of Paraná continental flood basalts of Santa Catarina state, southern Brazil. *Journal of Petrology* **26,** 187–209.

McKenzie, D. P. (1989). Some remarks on the movement of small melt fractions in the mantle. *Earth and Planetary Science Letters* **95,** 53–72.

McKenzie, D. P. & Bickle, M. J. (1988). The volume and composition of melt generated by extension of the lithosphere. *Journal of Petrology* **29,** 625–679.

Milner, S. C. & le Roex, A. P. (1996). Isotope characteristics of the Okenyenya igneous complex, northwestern Namibia: constraints on the composition of the early Tristan plume and the origin of the EM1 mantle component. *Earth and Planetary Science Letters* **141,** 227–291.

Milner, S. C., Duncan, A. D., Whittingham, A. M. & Ewart, A. (1995*a*). Trans-Atlantic correlation of eruptive sequences and individual silicic volcanic units within the Paraná–Etendeka igneous province. *Journal of Volcanology and Geothermal Research* **69,** 137–157.

Milner, S. C., le Roex, A. P. & O'Connor, J. M. (1995*b*). Age of Mesozoic igneous rocks in northwestern Namibia, and their relationship to continental break-up. *Journal of the Geological Society, London* **152,** 97–104.

Molzahn, M., Reisberg, L. & Wörner, G. (1996). Os, Sr, Nd, Pb, O isotope and trace element data from the Ferrar flood basalts, Antarctica: evidence for an enriched subcontinental lithospheric source. *Earth and Planetary Science Letters* **144,** 529–546.

Morgan, W. J. (1981). Hotspot tracks and the opening of the Atlantic and Indian Oceans. In: Emiliani, C. (ed.) *The Sea: The Oceanic Lithosphere*. New York: John Wiley, pp. 443–487.

O'Connor, J. M. & Duncan, R. A. (1990). Evolution of the Walvis Ridge–Rio Grande Rise hot spot system: implications for African and South American plate motions over plumes. *Journal of Geophysical Research* **95,** 17475–17502.

Peate, D. W. (1990). Stratigraphy and petrogenesis of the Paraná continental flood basalts, southern Brazil. Ph.D. Thesis, The Open University, Milton Keynes, UK.

Peate, D. W. & Hawkesworth, C. J. (1996). Lithospheric to asthenospheric transition in Low-Ti flood basalts from southern Paraná, Brazil. *Chemical Geology* **127,** 1–24.

Peate, D. W., Hawkesworth, C. J., Mantovani, M. S. M. & Shukovsky, W. (1990). Mantle plumes and flood basalt stratigraphy in the Paraná, South America. *Geology* **18,** 1223–1226.

Peate, D. W., Hawkesworth, C. J. & Mantovani, M. S. M. (1992). Chemical stratigraphy of the Paraná lavas (South America): classification of magma types and their spatial distribution. *Bulletin of Volcanology* **55,** 119–139.

Piccirillo, E. M. & Melfi, A. J. (1988). *The Mesozoic Flood Volcanism of the Paraná Basin: Petrogenetic and Geophysical Aspects*. São Paulo: IAG-USP Press.

Potts, P. J., Thorpe, O. W., Isaacs, M. C. & Wright, D. W. (1985). High precision instrumental neutron activation analysis of geological samples employing simultaneous counting with both planar and coaxial detectors. *Chemical Geology* **48,** 145–155.

Regelous, M. (1993). Geochemistry of dolerites from the Paraná flood basalt province, southern Brazil. Ph.D. Thesis, The Open University, Milton Keynes, UK.

Renne, P.R., Ernesto, M., Pacca, I.G., Coe, R.S., Glen, J.M., Prévot, M. & Perrin, M. (1992). The age of Paraná flood volcanism, rifting of Gondwanaland, and the Jurassic–Cretaceous boundary. *Science* **258,** 975–979.

Richardson, S. H., Erlank, A. J., Duncan, A. R. & Reid, D. L. (1982). Correlated Nd, Sr and Pb isotope variation in Walvis Ridge basalts and implications for the evolution of their mantle source. *Earth and Planetary Science Letters* **59,** 327–342.

Saunders, A. D., Storey, M., Kent, R. W. & Norry, M. J. (1992). Consequences of plume–lithosphere interactions. In: Storey, B. C., Alabaster, A. & Pankhurst, R. J. (eds) *Magmatism and the Cause of Continental Break-up. Geological Society, London, Special Publication* **68,** 41–60.

Storey, M., Mahoney, J. J. & Saunders, A. D. (1997). Cretaceous basalts in Madagascar and the transition between plume and continental lithosphere mantle sources. In: Mahoney, J. J. & Coffin, M. F. (eds) *Large Igneous Provinces: Continental, Oceanic, and Planetary Flood Volcanism. Geophysical Monograph, American Geophysical Union* **100,** 95–122.

Sun, S.-s. & McDonough, W. F. (1989). Chemical and isotopic systematics of oceanic basalts: implications for mantle compositions and processes. In: Saunders, A. D. & Norry, M. J. (eds) *Magmatism in the Ocean Basins. Geological Society, London, Special Publication* **42,** 313–344.

Sweeney, R. J., Duncan, A. R. & Erlank, A. J. (1994). Geochemistry and petrogenesis of central Lebombo basalts of the Karoo igneous province. *Journal of Petrology* **35,** 95–125.

Thirlwall, M. F., Upton, B. G. J. & Jenkins, C. (1994). Interaction between continental lithosphere and the Iceland plume: Sr–Nd–Pb isotope geochemistry of Tertiary basalts, NE Greenland. *Journal of Petrology* **35,** 839–879.

Thompson, R. N., Morrison, M. A., Dickin, A. P. & Hendry, G. L. (1983). Continental flood basalts ... Arachnids rule OK. In: Hawkesworth, C. J. & Norry, M. J. (eds) *Continental Basalts and Mantle Xenoliths*. Nantwich, UK: Shiva Press, pp. 158–185.

Todt, W., Cliff, R. A., Hanser, A. & Hofmann, A. W. (1996). Evaluation of a ^{202}Pb–^{205}Pb double spike for high precision lead isotopic analysis. In: Basu, A. & Hart, S. R. (eds) *Earth Processes: Reading the Isotopic Code. Geophysical Monograph, American Geophysical Union* **95,** 429–437.

Toyoda, K., Horiuchi, H. & Tokonami, M. (1994). Dupal anomaly of Brazilian carbonatites: geochemical correlations with hotspots in the South Atlantic and implications for the mantle source. *Earth and Planetary Science Letters* **126,** 315–331.

Turner, S., Regelous, M., Kelley, S., Hawkesworth, C. J. & Mantovani, M. S. M. (1994). Magmatism and continental break-up in the South Atlantic: high precision ^{40}Ar–^{39}Ar geochronology. *Earth and Planetary Science Letters* **121,** 333–348.

Turner, S., Hawkesworth, C. J., Gallagher, K., Stewart, K., Peate, D. W. & Mantovani, M. S. M. (1996). Mantle plumes, flood basalts and thermal models for melt generation beneath continents: assessment of a conductive heating model and application to the Paraná. *Journal of Geophysical Research* **101,** 11503–11518.

Ulbrich, H. G. J. & Gomes, C. B. (1981). Alkaline rocks from continental Brazil. *Earth-Science Reviews* **17,** 131–154.

Weaver, B. L., Wood, D. A., Tarney, J. & Joron, J. L. (1987). Geochemistry of ocean island basalts from the South Atlantic: Ascension, Bouvet, St. Helena, Gough and Tristan da Cunha. In: Fitton, J. G. & Upton, B. G. J. (eds) *Alkaline Igneous Rocks. Geological Society, London, Special Publication* **30,** 253–267.

White, R. S. & McKenzie, D. P. (1989). Magmatism at rift zones. *Journal of Geophysical Research* **94,** 7685–7730.

White, R. S. & McKenzie, D. P. (1995). Mantle plumes and flood basalts. *Journal of Geophysical Research* **100,** 17543–17585.

Wood, D. A., Gibson, I. L. & Thompson, R. N. (1976). Element mobility during zeolite-facies metamorphism of the Tertiary basalts of eastern Iceland. *Contributions to Mineralogy and Petrology* **55,** 241–255.

Zindler, A. & Hart, S. R. (1986). Chemical geodynamics. *Annual Review of Earth and Planetary Sciences* **14,** 493–523.